An Inquiry into Aspects of Fouling in a Diffusiophoretic Separation System

A Major Qualifying Project

Submitted to the Faculty of

Worcester Polytechnic Institute

In partial fulfillment of the requirements

For the degree in Bachelor's of Science

In

Chemical Engineering

By

Albert Foun

Sam Qu

Maheer Quasem

Date: April 27, 2023

Project Advisor: Professor Andrew R. Teixeira (CHE)

This report represents the work of WPI undergraduate students submitted to the faculty as evidence of a degree requirement. WPI routinely published these reports on its website without editorial or peer review. For more information about the projects program at WPI, see http://www.wpi.edu/Academics/Projects

Acknowledgements

This project would not have been possible without the tremendous amount of help we received from others. First and foremost, we are immensely grateful for the guidance and support from our project advisor, Professor Andrew R. Teixeira. We would also like to show appreciation to Ph.D. candidate Esai Lopez, for his daily assistance and mentorship in the lab. Additionally, we would like to thank all members of Professor Teixeira's Dynamics Lab for their encouragement and feedback. Lastly, we would like to thank Ian Anderson and Doug White for their time and expertise in determining appropriate methods to use and machining of parts when needed.

Abstract

Modern separation systems commonly use membranes or filters to trap and remove particles from mixtures or solutions. While effective, membrane separation systems can be energy intensive and require maintenance to replenish or replace membranes. Diffusiophoresis can be used to separate colloidal particles without the use of a fouling membrane; it does this by creating a concentration gradient with charged ions that drags particles in a certain direction. This approach allows for continuous separation that has the potential to be more cost and energy efficient. However, this technology is still being developed and has several gaps in research. One primary concern with a diffusiophoretic system is that physical limitations could inhibit separation efficiency and system practicality. Our team's goal was to investigate the physical phenomena associated with a tube-in-tube diffusiophoretic separation system used for separating polystyrene in water. This included experimental trialing of fouling under varying conditions as well as a computational study of particle tracing and velocity profiles within the system to enhance our understanding of mixing within the system. This report highlights the practical issues of constructing and maintaining the system and reports the accumulation over time when there is active diffusiophoresis versus no diffusiophoresis which revealed that less fouling occurred in the presence of diffusiophoresis.

Tables of Contents

Acknowledgements 2
Abstract 3
Tables of Contents 4
List of Figures 6
List of Tables 8
Technical Background 11
Diffusiophoresis 11
System 14
Fouling 18
UV-vis Spectroscopy 20
Materials and Methods 23
System and Cleaning 23
Calibration Curve 23
Flow Rate 26
Mass Balance 27
Experimental Runs 27
COMSOL Multiphysics 28
Fouling Experimentation Discoveries 30
Data Collection 30
Cleaning 35
COMSOL Simulations 40
Model Construction and Geometry 40
Physics Packages 41
Laminar Flow 41
Particle Tracing for Fluid Flow 42
Mesh 44
Results 45
Conclusions and Recommendations 50
Fouling 50
Mixing of Particles and Disturbances to Flow in the Gap Region 50
Recommendations for Future Works 51

References 53
Appendix A - Calculations 58
A.1: Volume of CO_2 Line 58
A.2: Volume of Water Line 58
A.3: Water Volume 58
A.4: Solution Flow Rate 58
A.4: Beer-Lambert Law 58
A.5: Mass Balance 59
Appendix B – Additional Plots 60
Appendix C – Additional Tables 62

List of Figures

Figure 1. Ions and their motion created from the reaction equations and diffusiophoresis process.[9] 12
Figure 2. Gas permeability coefficients vs. critical volume for Teflon AF-1600 and Teflon AF-2400. When observing the permeability coefficient for CO_2, AF-2400 demonstrates a higher value than AF-1600 concluding that AF-2400 is more essential for diffusiophoresis.[17] 16
Figure 3. Gas permeability of PDMS for CO_2 and He gas as a function of length. Reproduced from Firpo et al. [18] 17
Figure 4. Tube-in-tube setup for diffusiophoresis process to investigate fouling within the system. The outer lines represent the water line and the inner lines represent the CO_2 line. Table 2 demonstrates the sizing of the tubes. 17
Figure 5. General intensity versus wavelength plot with distilled water (DI water) as the sample. The sample was placed into a cuvette with a path length of 1 cm and had an integration time of 8.5 ms. The light values represent the intensity values when the light bulb shutter is open and the dark values represent the values when the shutter is closed to eliminate noise. 21
Figure 6. Example of theoretical versus measured calibration curve of a mixture between methanol and indocyanine green dye with a cuvette path length of 0.0763 um.[24] 22
Figure 7. A crack in the CO_2 line after attempting to assembly the system without the capillary. 23
Figure 8. Light source and cuvette utilized to obtain UV-vis intensity data for calibration curve and trials. 24
Figure 9. Transmission versus wavelength plots formed by Ocean Optics. The reference plot (left) is distilled water with no PS and the right plot contains distilled water mixed with PS to form a 66.67 $mg*L^{-1}$ solution. 24
Figure 10. Intensity versus wavelength plot from Ocean Optics data. The reference sample consisted of only distilled water (blue). The 66.67 $mg*L^{-1}$ sample consisted of polystyrene and distilled water mixture which had lower intensity values (gray). 25
Figure 11. Absorbance versus concentration calibration curve for polystyrene solution in 1 cm cuvette. For each trend line the slope of each line was used to determine the sample concentrations. 26
Figure 12. Schematic of the full system as described by Lyu, with parts being modeled using COMSOL such as the active zone and the gap region labeled.[9] 29
Figure 13. Initial flow cell utilized when attempting to collect UV data. 30
Figure 14. Flow cell data of 250 NTU polystyrene in water before and after a 24-hour trial. Using the same sample of polystyrene in water, the intensity measured after a trial was lower than the initial intensity indicating that fouling occurred in the flow cell. 31
Figure 15. Intensity curves of flow cell over water line. The DI water reference (left) demonstrates a curve we expected. However, with a capillary inserted into the water line (right), the intensity decreased slightly at the peak. If the water line were completely straight, all intensity values would have decreased significantly more as there would be major interference in the light's path. This trend demonstrates that the water line was not completely aligned with the flow cell and was not sufficient to use. 32
Figure 16. Particle build up over 24 hour period for a non-CO_2 and CO_2 system. 33
Figure 17. Pressure over time of the non-diffusiophoresis run. A pressure increase represents the formation of a clog in the system and a pressure decrease is due to the loss of a clog exiting out of the system. 34

Figure 18. Comparison of CO_2 line before (left) and after (right) running the system. The CO_2 line after the run has a spot of visible build-up, around 1.2 mm long. Where the before image is the CO_2 line after being cleaned in the ultrasonic cleaner. 35
Figure 19. 0.1 mg of polystyrene (bead) in 100 mL of acetone solution after 16 hours of mixing. The white substance in the middle of figure was the bead which had deformed and most likely formed napalm which is the product of mixing polystyrene and acetone. 36
Figure 20. 0.1 mg of polystyrene (dry) in 100 mL of acetone solution after an hour of mixing. From this chemical reaction, napalm is created which is a rubberish substance. 37
Figure 21. Deformed O-ring on metal syringe after letting acetone sit for an hour. 37
Figure 22. Comparison of water line before the run (left) and water line after the ultra-sonic cleaning (right). Water line was left in the ultra-sonic cleaner for 1 hour. DI water and air were then flown through the tubing to remove any excess water from the cleaner. 39
Figure 23. Schematics of the COMSOL model where the axis of symmetry represents the center of the tube, capillary, wall of the capillary, and the dirty outlet labeled. 40
Figure 24. Final mesh used in COMSOL with modifications with distribution near inlet and outlets, ratio of 1.2, corner refinement around the inlet and outlets, free triangular meshes, and finer mesh sizes. 45
Figure 25. The particle trajectories of 10 particles being released at t = 0 and with uniform distribution along the inlet (left). The surface plot of the velocity field in the domain with streamlines shown (right). 46
Figure 26. Normalized % of all particles released plotted against radial position in the gap region. 48
Figure 27. Pressure data of a no CO_2 run over 18 hour run time. Clearly shows pressure staying constant and then increasing over time demonstrating the formation of clogs over time. The decrease in pressure represents a clog leaving the system. 60
Figure 28. The number of particles across the outlets plotted against the radial position with an initial release of 100,000 particles. 60
Figure 29. The number of particles across the outlets plotted against the radial position with an initial release of 50,000 particles. 61

List of Tables

Table 1. Chemical reactions occurring during diffusiophoresis from the mixing of CO_2 and water. 12
Table 2. Measurement details of inner and outer tubing used for system. 18
Table 3. Fouling categories based on size 19
Table 4. Experimental settings for diffusiophoretic system. 28
Table 5. Summary of parameters used and operating conditions used for this simulation. 41
Table 6. Reported values of initial particles released, resulting number of particles at the clean withdraw and dirty outlet and percentages for both. 47
Table 7. Absorbance and outlet concentration data for no CO2 run at a wavelength of 356.819 nm. The outlet concentration was converted to accumulation with the use of the mass balance to create Figure 16. 62
Table 8. Absorbance and outlet concentration data for CO2 run at a wavelength of 356.819 nm. The outlet concentration was converted to accumulation with the use of the mass balance to create Figure 16. 62

Introduction

Water makes up around 1,368 million km^3 of Earth's hydrosphere, however, only 2.5% of this water is fresh and acts as viable drinking water for the global population, resulting in freshwater being an important resource.[1] If a negative impact were to happen to water sources, resulting in the presence of pollutants and contaminants in the world's supply of water, its necessary that those issues be fixed as soon as possible.[2] In order to rid of pollutants and contaminants in water streams, water filtration methods have been developed to separate particles and water. One method commonly used is reverse osmosis which utilizes a membrane to "reject" and act as a barrier to contaminants.[3]

An alternate method to water separation is through diffusiophoresis. Diffusiophoresis does not rely on using a membrane to separate particles from the stream but relies on the formation of chemical gradients.[4] During the suspension, the particles are able to move due to the creation of a concentration gradient from the use of carbon dioxide (CO_2) and the contact between solute and solutions.[5] In the diffusiophoretic system, permeable tubing allows for the CO_2 to react with water and produce ions that induce the concentration gradient.[6] The lack of a membrane results in the need for less energy consumption and increase the efficiency in portability.[7]

Whether the water filtration process uses a membrane or not, a common trend that occurs is the creation of foulants in the system due to the particles in the stream. Foulants can cause major problems to the system as they can cause damage and cause performance to decrease over time. As a result, more time and money is spent on maintaining the system properly.[3]

Due to little research on the subject of fouling in a diffusiophoretic system, our objective is to determine various conditions that impact fouling when using diffusiophoresis. In addition, we plan to determine how fouling impacts the apparatus. These objectives will be achieved by running the

same concentration of polystyrene (PS) in water solution through a diffusiophoretic and non-diffusiophoretic system. Both systems will operate under a constant residence time and run time. The amount of buildup in the system will be determined through the use of a UV-vis cuvette which will determine the outlet concentration and a mass balance will calculate the amount of accumulation in the system. In addition to testing the system, a computer simulation utilizing COMSOL will be used to predict the system behavior and determine the split ratio at the "gap" between the CO_2 line and capillary. This paper will go over background information on the theory of diffusiophoresis and fouling. In addition, the systems tube-in-tube design will be discussed. The materials utilized and our main method steps will be further discussed in the Materials and Methods section. The results section will demonstrate the data collected from the experiment such as accumulation over system time run and the discussions section will further interpret and analyze our results. Lastly, the conclusions and recommendation section will discuss possibilities to further improve and understand diffusiophoretic fouling experiments.

Technical Background

Diffusiophoresis

Diffusiophoresis occurs from the gradients created from electrophoresis and chemiphoresis which act as the driving forces. When the solution of charged particles is sent through the system, an electric field is induced from the difference in ion diffusivities which contribute to electrophoresis. Chemiphoresis occurs from "osmotic pressure imbalances" between the particles and fluid region. The combination of electrophoresis and chemiphoresis create a concentration gradient and induce particle motion. The diffusiophoretic velocity of the particles can be calculated as shown in Equation 1.

$$u_{dp} = \left(\Gamma_{cp} + \Gamma_{ep}\right)\nabla \ln c \qquad (1)$$

In the equation, u_{dp} is the "particle diffusiophoretic velocity," c is equivalent to the concentration of the solute, Γ_{cp} and Γ_{ep} represent the chemiphoretic and electrophoretic diffusiophoretic mobilities, respectively.[9] In the presence of non-electrolytic feeds and particles, electrophoresis does not take effect and diffusiophoresis relies on only chemiphoresis. This is due to the particles being non-electrolytic which does not allow for the diffusivities to create an electric field.[8]

In the system, chemiphoresis and electrophoresis occur from the interactions of the solution and use of carbon dioxide. CO_2 dissociate in water which creates ions that induce the phenomenon. When using semi-permeable material, such as Teflon AF-2400, for the system, CO_2 is able to permeate into water and react. This reaction leads to the creation of positively charged hydrogen ions (H^+) and negatively charged carbonate ions (CO^{2-}_3). The chemical reactions that occur in the system can be shown in Table 1 and the motion of the products can be shown in Figure 1.[6]

Table 1. Chemical reactions occurring during diffusiophoresis from the mixing of CO_2 and water.

	Equilibrium Equation
(1)	$CO_2(g) + H_2O\ (l) \leftrightarrow H_2CO_3(aq)$
(2)	$H_2CO_3(aq) \leftrightarrow HCO_3^-(aq) + H^+(aq)$
(3)	$HCO_3^-(aq) \leftrightarrow CO_3^{2-}(aq) + H^+(aq)$

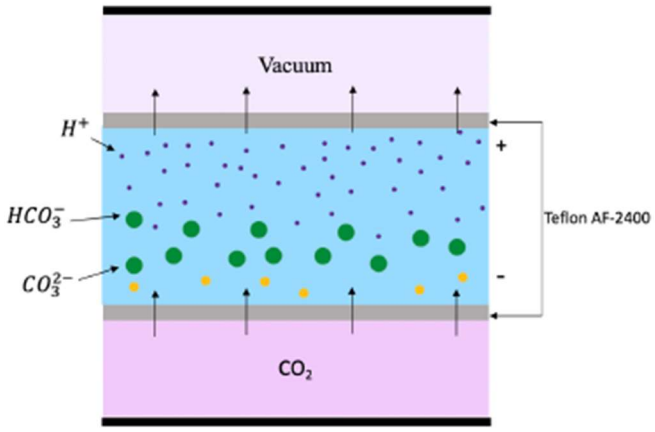

Figure 1. Ions and their motion created from the reaction equations and diffusiophoresis process.[9]

From the reaction of CO_2 and water, H^+ ions are created and negatively charged polystyrene particles, caused from the aromatic ring, interact in the system which causes a concentration gradient to form from the large diffusivity difference among the ions.[5] As a result, the negatively charged particles will depend on the positively charged ions and move accordingly. The concentration of polystyrene is expected to decrease over the axial length of the system and will vary from various parameters.[10]

The migration and flow of the particles induced by chemiphoresis and electrophoresis can be impacted by adjusting specific parameters such as flow rate, diffusivity, geometry, etc. The dimensionless Sherwood number can determine the "natural ion depletion and diffusiophoretic exclusion" that occurs in the system. As shown in Equation 2, the Sherwood number can be calculated and varied based on certain parameters.

$$Sh = \left[\frac{\left(\frac{W}{L_n}\right)(c_0 U_{mean})}{\left(\frac{D_{eff} c_0}{W}\right)}\right] = \frac{W^2 U_{mean}}{L_n D_{eff}} \quad (2)$$

When solving for the Sherwood number (Sh), W is the microchannel "half-width," U_{mean} is the average velocity of the flow, L_n is the horizontal distance of the medium, and D_{eff} is the effective diffusivity of the particles. Equation 2 more so closely resembles the Peclet number however, the equation utilizes the "boundary flux scale." This was done due to the Peclet number the diffusion rate not incorporating "ion exchange interface" diffusive flux. The Sherwood number was then found by multiplying the "channel aspect ratio" by the "convective transfer" in the vertical direction. This value was then divided by the "ion exchange interface" boundary, as shown in Equation 2.[11]

Another factor that can impact diffusiophoresis is the diffusivity difference between ions. Due to diffusiophoresis being reliant on an induced electric field from the solute, the ion diffusivity difference can impact the effect of electrophoresis. Beta (β) represents the difference between the cation and anion diffusivities as shown in Equation 3.

$$\beta = \frac{(D_+ - D_-)}{(D_+ + D_-)} \quad (3)$$

In this equation, D_+ and D_- are the diffusivities of the cation and anion, respectively. An induced electric field can be determined from the beta value, concentration gradient, temperature, and etc. as shown in Equation 4.

$$E = \frac{kT}{Ze} \beta \frac{\nabla C}{C} \quad (4)$$

In the induced electric field equation, k is the Boltzmann constant, Z is the "valence of the constituent ions of solute," T is the temperature of the system, e is the "proton charge," ∇C is the

concentration gradient, and C is the concentration of the ions. When substituting Equation 3 into Equation 4, Equation 5 demonstrates all the factors the electric field. Based on this equation, the diffusivities and concentration gradient can heavily impact the induced electric which in turn would impact the effect of electrophoresis and diffusiophoresis.[12]

$$E = \frac{kT}{Ze}\left(\frac{(D_+ - D_-)}{(D_+ + D_-)}\right)\frac{\nabla C}{C} \quad (5)$$

In order to determine the diffusivity of the cation and anions throughout the system, the Stokes-Einstein equation is utilized as shown in Equation 6.

$$D = \frac{kT}{6\pi\eta a} \quad (6)$$

In the Stokes-Einstein equation, D represents the diffusivity, k is the Boltzmann's constant, T is the temperature, η is the dynamic viscosity, and α is particle radius. From this equation, the diffusivity factor can be determined.[12]

System

Tube-in-tube reactors have been discussed for use in flow chemistry applications. In these cases, there would be two tubes of various sizes, constructed with a concentric geometry, where the inner tube would be gas permeable. Doing so allows diffusion of gas through the semi-permeable material without the two phases directly coming into contact. For the diffusion process, "small diffusion" lengths are achieved due to "rapid gas-liquid mass transfer rates".[13] This setup is useful in situations where the behavior of the interface needs to be "well-defined," such as measuring the gas solubility in a liquid.[14]

Teflon AF-2400 is used as the tubing material for the separation process due to the chemical makeup. Teflon AF-2400 consists of tetrafluoroethylene (C_2F_4) and

perfluorodimethyldioxolane monomers, which link together to form a copolymer, which result in the optimal conditions for liquids and gases to interact with one another. The copolymer tubing allows for no liquid permeability and majority of gas permeability to occur in the system. The gas permeability are due to the diffusion coefficients of the species being relatively high, which leads to more diffusion to occur, demonstrating and allowing gas molecules with a small radius and size are most likely to permeate through the material.[15] This would allow the CO_2 to permeate through the tubing and react with water. In addition, water would not be able to permeate through the tubing and enter the CO_2 line.[16]

Teflon AF-2400 was chosen for the tubing material due to its CO_2 gas permeability capabilities. Other potential materials that could have been used for the system include Teflon AF-1600 and Polydimethylsiloxane (PDMS). Teflon AF-1600 was not chosen due to having a lower CO_2 gas permeability than Teflon AF-2400. While a known value was not given for the CO_2 gas permeability by the official Teflon website, numerous studies have shown that Teflon AF-1600 has a lower permeability than Teflon AF-2400. One study done observed the gas permeability coefficients of Teflon AF-1600 and Teflon AF-2400 over various critical volumes for different gases as shown in Figure 2. Based on the figure, Teflon AF-2400 had the largest gas permeability coefficients than Teflon AF-1600 for each of the gasses and had the closest permeability coefficient to CO_2, demonstrating Teflon AF-2400 being a better choice for the system.[17]

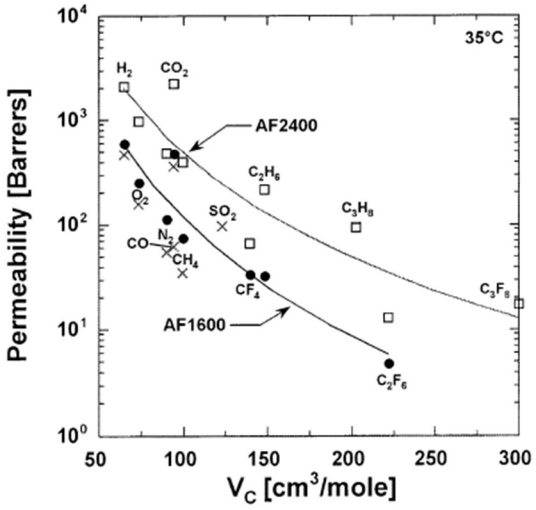

Figure 2. Gas permeability coefficients vs. critical volume for Teflon AF-1600 and Teflon AF-2400. When observing the permeability coefficient for CO_2, AF-2400 demonstrates a higher value than AF-1600 concluding that AF-2400 is more essential for diffusiophoresis.[17]

While Teflon AF-1600 has a lower permeability than Teflon AF-2400, PDMS generally has a slightly higher CO_2 gas permeability than Teflon AF-2400. A study measured the gas permeability of PDMS when using CO_2 and helium based on the length of the material. Based on the study, the gas permeability of PDMS after a length of 50 μm (0.05 mm) was determined to be independent and averaged around a permeability value of $1.0*10^{-12}$ mol^1 m^{-1} s^{-1} Pa^{-1}, as shown in Figure 3.[18] From the official Teflon website, the recorded permeability of Teflon AF-2400 to be equal to 2800 Barrer which is equivalent to $9.4*10^{-13}$ mol^1 m^{-1} s^{-1} Pa^{-1}, demonstrating PDMS having a slightly higher permeability.[19] However, due to the thickness of PDMS, Teflon AF-2400 was chosen over PDMS was due to their physical functionalities. PDMS is capable of "swelling" when used with toluene and acetone unlink Teflon AF-2400. In addition, PDMS does not have "mechanical strength" unlike Teflon AF-2400.[20]

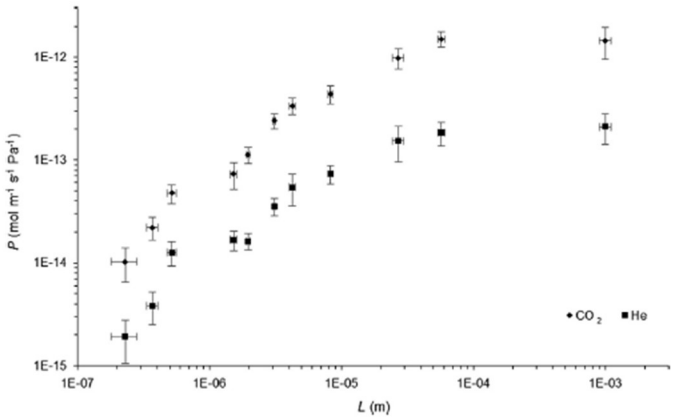

Figure 3. Gas permeability of PDMS for CO_2 and He gas as a function of length. Reproduced from Firpo et al. [18]

Due to Teflon AF-2400 having the potential to be non-porous, a "chemical potential gradient" can allow for gas and liquids to permeate through the material. A gas is able to permeate through the material due to the "downstream side" having a lower pressure than the "permeated species" vapor pressure.[21] This process would best represent diffusiophoresis separation as the tubing used in the process is non-porous as shown in Figure 4. Lastly, Teflon AF-2400 is a fluoroplastic which allows the material to have a "high resistance" to dangerous chemicals and in addition cause these chemicals to be inert.[19]

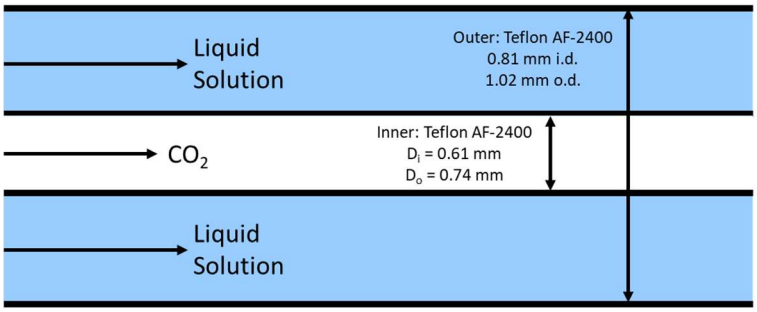

Figure 4. Tube-in-tube setup for diffusiophoresis process to investigate fouling within the system. The outer lines represent the water line and the inner lines represent the CO_2 line. Table 2 demonstrates the sizing of the tubes.

Table 2. Measurement details of inner and outer tubing used for system.

Line Type	Inner Diameter (mm)	Outer Diameter (mm)	Length (mm)
CO_2	0.6096	0.7366	40
Water	0.8128	1.0160	254.0
Capillary	0.4000	0.5000	-

Fouling

Fouling is the occurrence of particle accumulation and buildup on the membrane of most water separation processes. Fouling can cause major damage to a system due to the buildup causing increases pressure, maintenance, cleaning costs, and non-operational times while there are decreases in flow, flux, and productivity. Based on various factors, there are a number of factors that influence the type of fouling that occurs. These factors include temperature, feed water composition, flow velocity, membrane characteristics, etc. Generally there are two types of fouling, reversible and irreversible. Reversible fouling occurs when the membrane of the separation process rejects a "concentration polarization of materials." This concentration polarization is caused by the flux of water and mass transfer principles which induce the solute concentration to increase near the membrane and generally be larger than the bulk solution. Irreversible fouling occurs from the pore of the membrane begin to be plugged by the particles in the stream due to chemiphoresis.[22]

The type of foulants in the system are reliant on the feed composition. The four common types of foulants are organic, inorganic, micro-biological, and particulates. Based on the type of foulants that are in the system, the fouling mechanism can vary between cake formation, inorganic precipitation, biological fouling, organic adsorption, concentration polarization, and pore blocking. Particle and colloidal fouling rely on the size of the particles that are entering the system.

The sizing of the particles can be categorized to determine the type of particles as shown in Table 3.[22]

Table 3. Fouling categories based on size.

Category	Size
Settleable solids	> 100 μm
Supra-Colloidal solids	1 μm to 100 μm
Colloidal solids	0.001 μm (10 Å) to 1 μm
Dissolved solids	< 10 Å

If the system and membrane are not equipped with the correct material and pore sizing, particle and colloidal fouling can be expected as blockage may occur. For a nonporous membrane, buildup may occur and form a cake layer which would cause resistance to the feed flow. Organic fouling consists of three subcategories that include refractory natural organic material, synthetic organic compounds, and soluble microbial products.[22]

Due to the system utilizing diffusiophoresis as the main method of separation, fouling occurs through a different method than fouling with the use of a membrane. When diffusiophoresis is used, the "vortex breakdown phenomenon" causes particles from the feed to be trapped in the junctions that connect to the channels in the system. The particles are trapped due to the particle densities being less than the densities of the flowing fluid. In addition to the densities, the gradients created from electrophoresis and chemiphoresis play a role in the buildup.[23]

Fouling has been shown to occur in two different types of separation systems, a membrane and diffusiophoresis. However, there is a potential possibility that a combination both type of

separations are likely to occur within the same system and potentially increase fouling. An experiment was performed to measure fouling with the use of a reverse osmosis system while diffusiophoresis was active. From the experiment, the Guha and their team utilized salts which would induce diffusiophoresis from the diffusivity of the ions while there was a membrane used for reverse osmosis. The results of the experiment found that as the ion diffusivities decreased, the cake layer forming increased on the surface of the membrane. In addition, the team discovered that that the cake porosity and permeate velocity in the system impacted fouling caused by diffusiophoresis. The team was able to conclude that a reverse osmosis separation system would be able to induce diffusiophoresis and as a result increase the amount of fouling that can in the system which would further cause further implications for future runs.[3]

UV-vis Spectroscopy

UV-vis spectroscopy is an analytic method utilized to detect the absorbance and transmittance of light through a sample solution. For absorbance, ultra violet light is utilized for samples that rely on dissolution while samples that rely on suspension utilize visible light and transmittance. The wavelength range for ultra violet light is between 200 nm and 400 nm while visible light is between 400 nm and 800 nm.

A spectrophotometer is used for spectroscopy and works by shining a light, from a light source, through a sample and then this light shined through the sample is detected from a detector on the other side of the sample. From the detector, a plot of absorbance or intensity, no units, versus the wavelength, in nanometers, is created as shown in Figure 5. As seen, the sample generates a specific plot which is then compared to a reference sample.

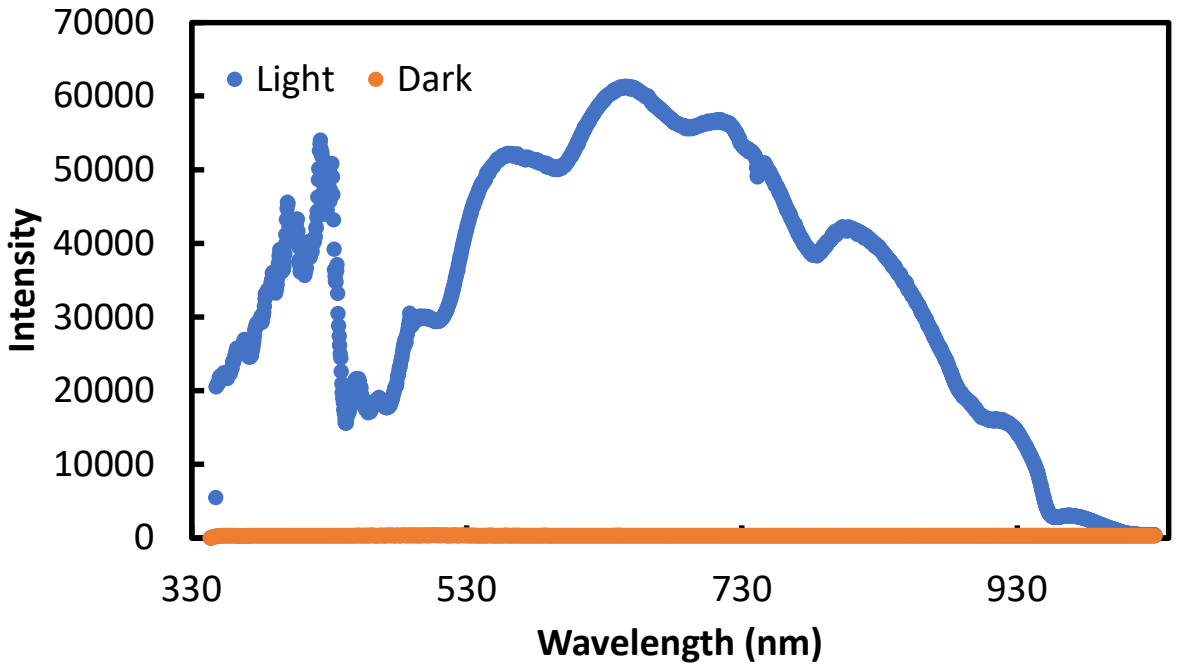

Figure 5. General intensity versus wavelength plot with distilled water (DI water) as the sample. The sample was placed into a cuvette with a path length of 1 cm and had an integration time of 8.5 ms. The light values represent the intensity values when the light bulb shutter is open and the dark values represent the values when the shutter is closed to eliminate noise.

The theory behind uv-vis spectroscopy comes from the transition of electrons. When light is absorbed by the solutions, the solution electrons are excited, due to the light, to a "higher energy unoccupied orbital." The Beer-Lambert law demonstrates the general theoretical trend of absorbance versus wavelength plot. The Beer-Lambert law is shown in Equation 7.

$$A = log_{10}\frac{I_0}{I} = \epsilon bC \qquad (7)$$

In this equation, I_0 is the intensity of the reference and I is the intensity of the sample. In addition, b is the path length which is the length at which is going through the sample, C is the concentration of the sample, and ε is the molar absorptivity constant which varies for every compound and vary at every wavelength. Since the absorbance varies with concentration, a theoretical calibration

curve can be created. From this theoretical plot, the measured values of absorbance can be compared to the theoretical as shown in Figure 6.[24]

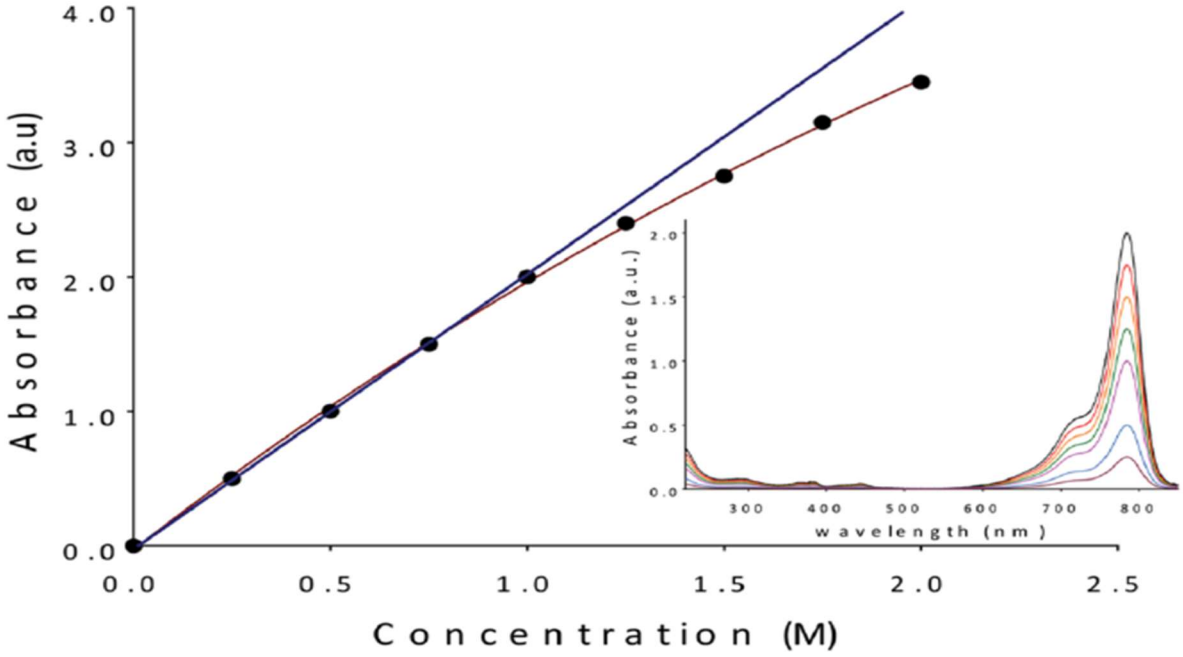

Figure 6. Example of theoretical versus measured calibration curve of a mixture between methanol and indocyanine green dye with a cuvette path length of 0.0763 um.[24]

Materials and Methods

System and Cleaning

In order to study the effects of diffusiophoresis on fouling in a tube in tube system, a system was constructed using two sizes of Teflon AF-2400 tubing. The inner tubing contained carbon dioxide while the outer tube contained flowing polystyrene and water solution. In addition to the tubing, a capillary was used to help diminish damage to the CO_2 line from bending and twisting. A result of not utilizing the capillary and tearing in the CO_2 line can be seen in Figure 7.

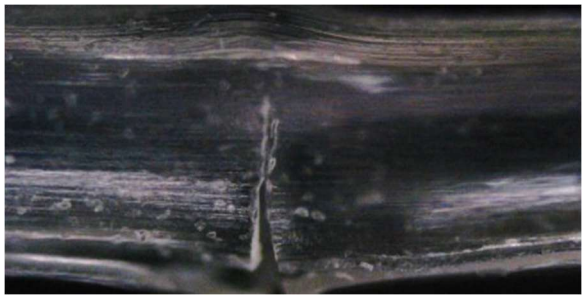

Figure 7. A crack in the CO_2 line after attempting to assemble the system without the capillary.

Utilizing the permeable tubing would allow CO_2 and water to react and form ions that will create concentration gradients. Once the run was done, the system was cleaned with an ultrasonic cleaner which would remove the buildup out of the tubing through mechanical vibration and cavitation.[25]

Calibration Curve

In order to monitor the change in the outlet concentration and determine the accumulation inside the system, UV-vis spectroscopy was used. By analyzing the outlet of each run in the spectrophotometer and determining the absorbances at various peak wavelengths, we plotted the absorbances on a calibration curve which could output the concentration of the sample. The calibration curve was created by creating various concentrations of polystyrene in water, ranging from 0 $mg*L^{-1}$ to 66.67 $mg*L^{-1}$, and placing 1 mL samples in a cuvette. The 0 $mg*L^{-1}$ sample was used as a reference sample for the rest of the known concentration samples. The cuvette was placed

into a cuvette holder, that has a path length of 1 cm, which would allow the light from the Ocean Optics light source to shine through the known concentration samples to a detector as shown in Figure 8.

Figure 8. Light source and cuvette utilized to obtain UV-vis intensity data for calibration curve and trials.

For each concentration, transmittance versus wavelength plots were graphed from Ocean Optics. A reference, distilled water, was expected to have a transmittance of 100% due to no impurities obstructing the light path through the cuvette. Once a solution with polystyrene was placed in the cuvette, the transmittance decreases due to particles suspending and interfering with the light. Figure 9 demonstrates the plots Ocean Optics developed while using the spectrometer.

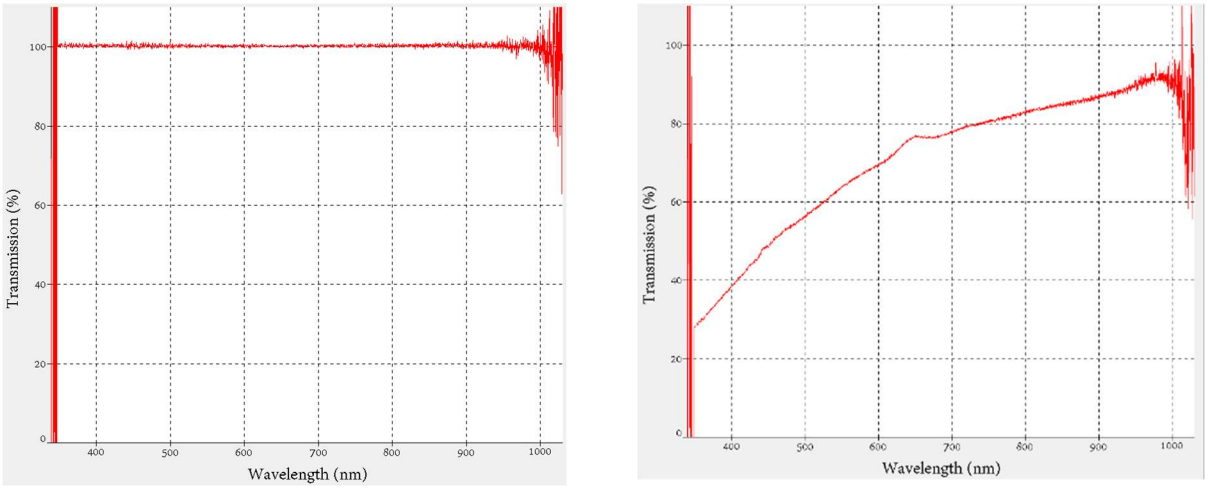

Figure 9. Transmission versus wavelength plots formed by Ocean Optics. The reference plot (left) is distilled water with no PS and the right plot contains distilled water mixed with PS to form a 66.67 $mg*L^{-1}$ solution.

In addition to the transmittance versus wavelength plots, an intensity versus wavelength plot, for each concentration, was created from Ocean Optics as shown in Figure 10. The reference sample of distilled water expected to have the highest intensity values and saw the intensity values decrease when increasing the concentration of the samples. This was due to the particles in the solution obstructing light so less light would exit the cuvette.

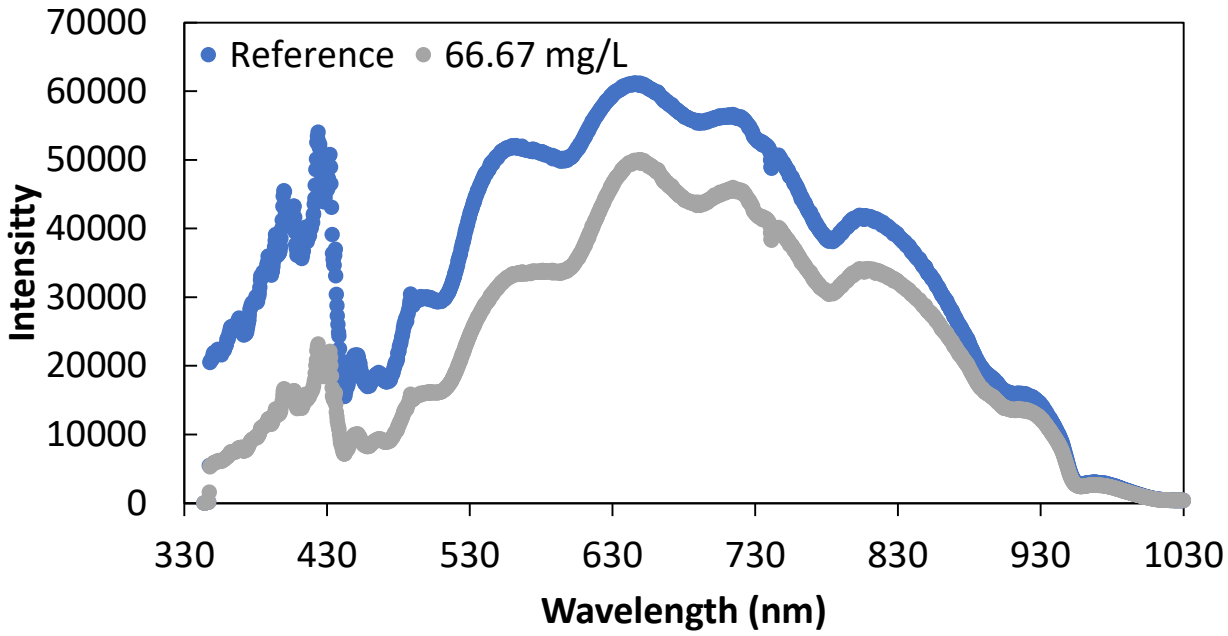

Figure 10. Intensity versus wavelength plot from Ocean Optics data. The reference sample consisted of only distilled water (blue). The 66.67 mg*L^{-1} sample consisted of polystyrene and distilled water mixture which had lower intensity values (gray).

From the intensity versus wavelength plots and reference plot, the absorbance versus wavelength plot could be created with Equation 8 and the intensity values. This equation is from the Beer-Lambert law and the Ocean Optics user manual.

$$A = -\log\left(\frac{I - I_{dark}}{I_{light} - I_{dark}}\right) \quad (8)$$

In this absorbance equation, I is the intensity of the sample, I_{dark} is the intensity of the reference when the opening to the light source is closed, and I_{light} is the intensity of the reference when the

opening is open. The dark intensity was taken to account for noise that may occur when light was shined through the sample.[26] The calibration curve was created three times with using the same samples made on the same days. Figure 11 demonstrates the calibration curve created from the average of the absorbances with the slope and R^2 values of the lines of best fit based on the wavelengths and samples measured.

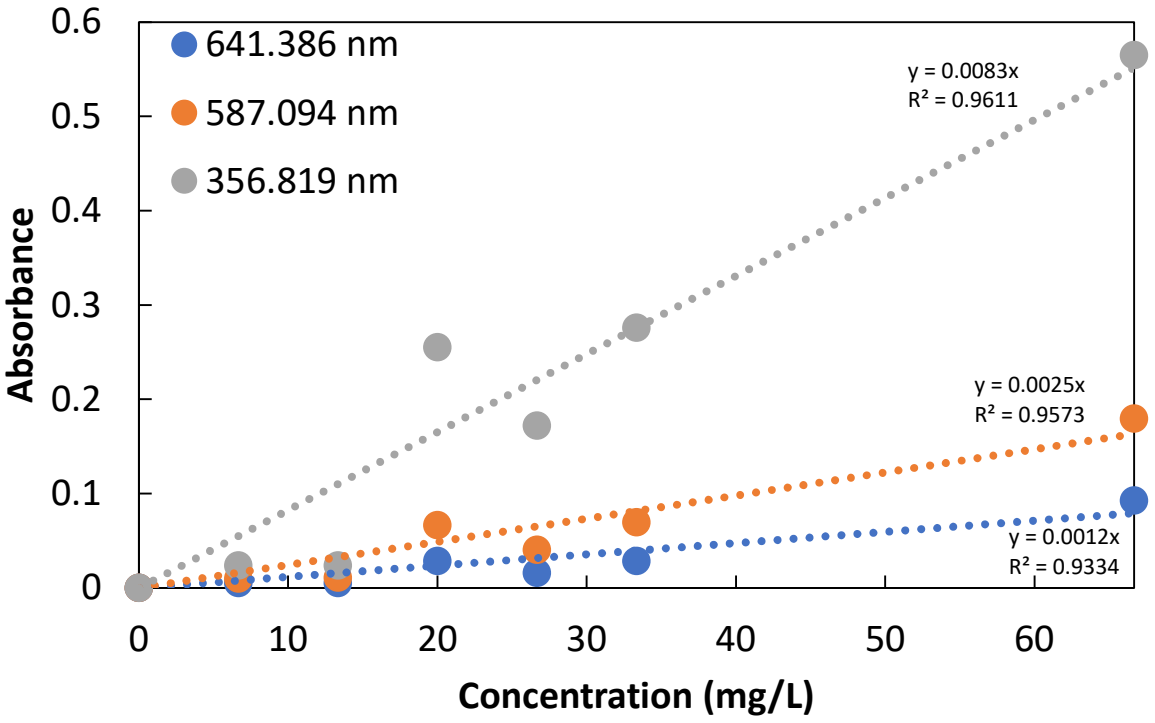

Figure 11. Absorbance versus concentration calibration curve for polystyrene solution in 1 cm cuvette. For each trend line the slope of each line was used to determine the sample concentrations.

Flow Rate

As the set inlet flow rate was inversely proportional to the residence time of particles in the system, adjusting the flow rate would effectively change the residence time. In doing so, the effects of residence time on the system, such as buildup of polystyrene particles and potential fouling can be studied. The flow rate was found and calculated based on Equation 9.

$$F = \frac{V_{H2O}}{t_{res}} \quad (9)$$

In this equation, F is the flow rate, V_{H2O} is the water volume between the water line and CO_2 line, and t_{res} is the residence of the system. For the study, a constant residence time of 75 seconds was utilized to ensure consistency between trials. The water line volume and solution flow rate calculations are shown in Appendix A.4.

Mass Balance

In order to determine the accumulation inside the system, we developed an equation based on a material balance around the system. The material balance can be seen in Equation 10 which is then further developed into Equation 11. The derivation and assumptions made for the full derivation can be seen in Appendix A.5.

$$Inlet - Oulet = Accumulation \quad (10)$$

$$Ft(x_{in} - x_{out}) = M \quad (11)$$

In the final PS mass balance equation, F is the flow rate of fluid that is set by the pump settings, x_{in} and x_{out} are the concentrations of the inlet and outlet samples, t is the run time, and M is the amount that accumulated over the run time.

Experimental Runs

To determine how run time and diffusiophoresis impacts fouling in the system, 2 trials were performed as shown in Table 4. As seen in Table 4 below, the initial concentration of the inlet solution was constant as 51.4 $mg*L^{-1}$ as this was used as a baseline. In addition to the inlet concentration staying constant, the residence time was kept constant at 75 s to ensure run time and diffusiophoresis impacts on fouling could be easily observed. Every three hours samples were collected until the 24 hour run time had completed. For each run, around 1 mL of each sample had

been drawn into a pipet and then placed into a cuvette where UV-vis intensity data was collected and recorded for wavelengths at 356.819, 587.094, and 641.386 nm. The absorption data collected was compared to the calibration data and graphs which determined the concentration of the outlet stream.

Table 4. Experimental settings for diffusiophoretic system.

Initial Concentration (mg L^{-1})	**Residence Time (s)**	**Run Time (hr)**	**CO_2 Pressure (kPag)**
51.5	75	24	0 250

COMSOL Multiphysics

Besides focusing on the effects of various parameters have on fouling in the active zone of the system experimentally, we also completed simulations of the downstream region immediately after the end of the active zone. As a method that is more cost and time efficient than running experiments in lab, COMSOL Multiphysics was used to predict expected behavior of certain parts of the system.

As the polystyrene particles are shown to move towards the wall of the water line as a result of diffusiophoresis, making the center of the flow relatively less concentrated. To obtain the water in the center of the flow, Lyu has shown the method of using a capillary, connected to a pump that is actively withdrawing from the system, placed near the end of the CO_2 line where it is plugged works.[9] However, there would need to be a gap between the capillary and the end of the CO_2 line. Having such a gap, or in other words, a sudden expansion in the flow path, which could risk unexpected behavior in particle motion. The simulations mainly focus on the particle flow path and velocity profile in the gap region between the capillary and the end of the CO_2 line where it's

plugged as shown in Figure 12. The purpose of this model was to prove our hypothesis that there is no mixing or disturbance to flow paths in the gap. The software used was COMSOL Multiphysics 6.0, which allows for easy changes in parameters, physical conditions, boundary and initial conditions, and system geometry.

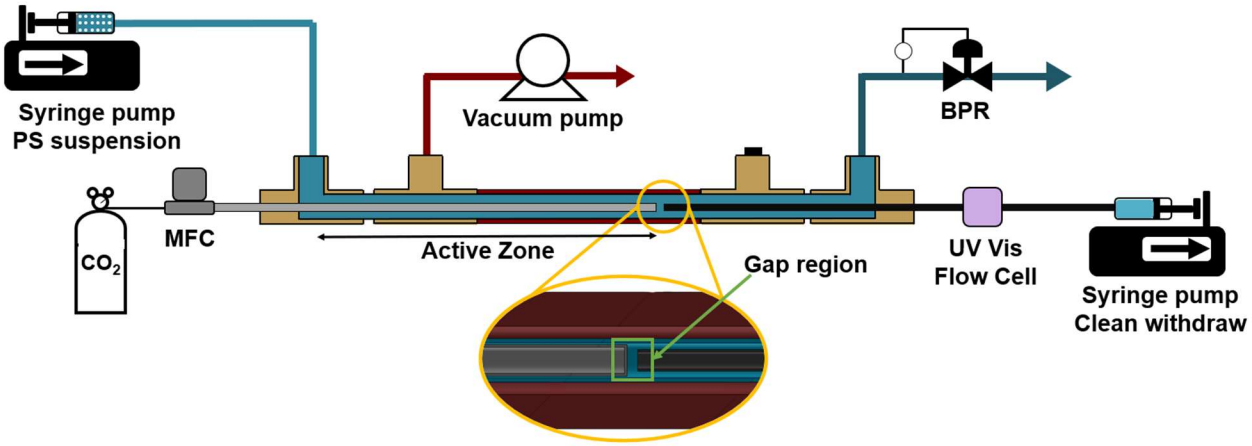

Figure 12. Schematic of the full system as described by Lyu, with parts being modeled using COMSOL such as the active zone and the gap region labeled.[9]

Fouling Experimentation Discoveries

Data Collection

To quantify the accumulation occurring within the diffusiophoretic system, two methods were used to collect concentration data of the system outlet. The first method involved using a UV-Vis Flow Cell, as shown in Figure 13, to collect transient wavelength data that could be translated into concentration data. This worked by attaching a flow cell at the end of the system to record absorbance as the mixture flows through the tubing. Through collecting continuous outlet data, it would be possible to study the separation and fouling occurring in the system at specific times and develop an accurate accumulation versus time plot.

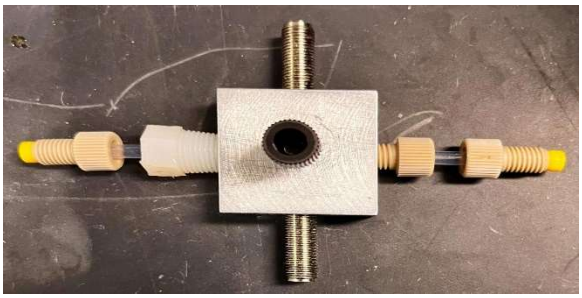

Figure 13. Initial flow cell utilized when attempting to collect UV data.

Although this method created a larger set of data and allowed the system to be left alone during experimental trials, several issues affected the validity of the flow cell results. First, after running several trials, we noticed that the intensity reading of the flow cell decreased over time even when the same sample was pumped through the system. To verify that the change in intensity was due to concentration, we tested the same sample of polystyrene in water both before the experiments and after using only the flow cell detached from the system. As shown in Figure 14, the same sample after the experiments yielded a lower intensity. This indicates that during the trials, fouling was occurring not only in the system but in the flow cell as well. This made it impossible to distinguish changes in absorption because of concentration changes versus changes due to accumulation in the flow cell.

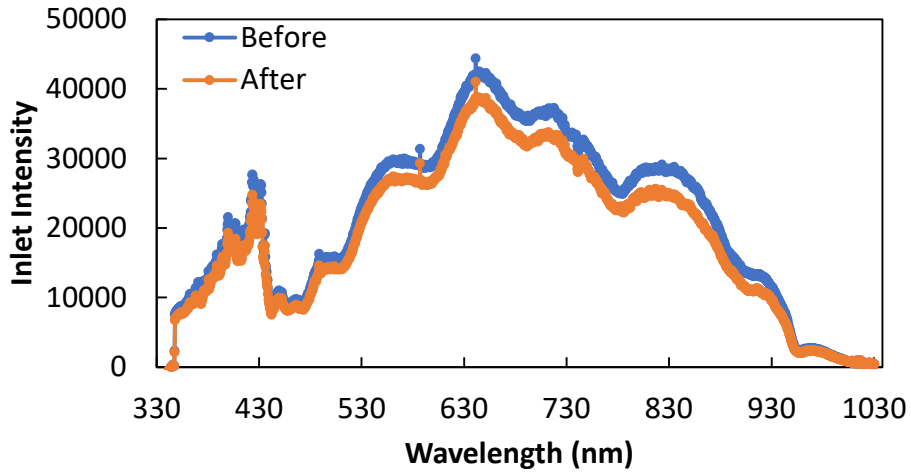

Figure 14. Flow cell data of 250 NTU polystyrene in water before and after a 24-hour trial. Using the same sample of polystyrene in water, the intensity measured after a trial was lower than the initial intensity indicating that fouling occurred in the flow cell.

To resolve the flow cell fouling issue, we attempted to attach the flow cell directly to the system, attaching it to the water line directly after the diffusiophoretic active zone. However, another issue occurred involving the alignment of the tubing in the flow cell. To obtain an accurate reading, we needed the water line to pass through the center of the flow cell so that the light for the spectrometer would cross through the water tubing. However, in the process of securing the flow cell to the system, tightening the ferrules on each end of the flow cell caused a flex in the tubing which offset the path, allowing for light to pass directly through to the spectrometer without interference from the line and mixture. To verify these results, we looked at the flow cell data both with empty tubing and a metal capillary in the tubing. In theory, the solid metal capillary should block most of the light if the flow cell was properly aligned on the system. However, as shown in Figure 15, the intensities between the two tests did not reveal expected differences compared to how much light the capillary should have blocked. This indicated that the flow cell was not properly reading the contents of the system tubing thus making the data invalid.

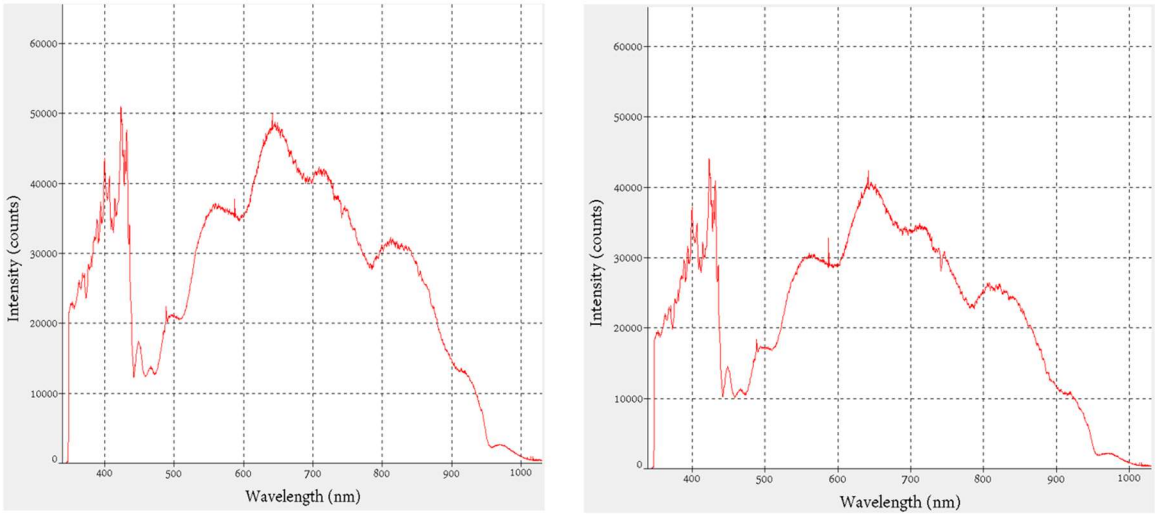

Figure 15. Intensity curves of flow cell over water line. The DI water reference (left) demonstrates a curve we expected. However, with a capillary inserted into the water line (right), the intensity decreased slightly at the peak. If the water line were completely straight, all intensity values would have decreased significantly more as there would be major interference in the light's path. This trend demonstrates that the water line was not completely aligned with the flow cell and was not sufficient to use.

After attempting to utilize the UV-flow cell, our final collection method relied on batch sampling. Batch sampling was chosen as the main method due to no fouling occurring over time when analyzing the data. Every 3 hours, samples of the outlet were taken and placed into the cuvette where light would shine through the cuvette until 24 hours had taken place.

Initially, we expected that as the outlet concentration would generally decrease over time due to theorized accumulation inside the system. Thus, from the mass balance, the accumulation would demonstrate a positive trend. In addition to the general trend, we expected the fouling to increase when diffusiophoresis was active due to the idea that the concentration gradient would cause more particles to accumulate over time compared to no diffusiophoresis active.

After analyzing and recording the outlet sample intensities for various wavelengths, the wavelength of 356.819 nm was chosen due to its linear regression R^2 value being closest to the 1 demonstrating the most linear trend out of the three wavelengths as shown in Figure 11. Once the

outlet intensities were recorded and the concentrations were found from the calibration curve, the mass balance determined the amount of particles that built up over the 24 hours as shown in Figure 16.

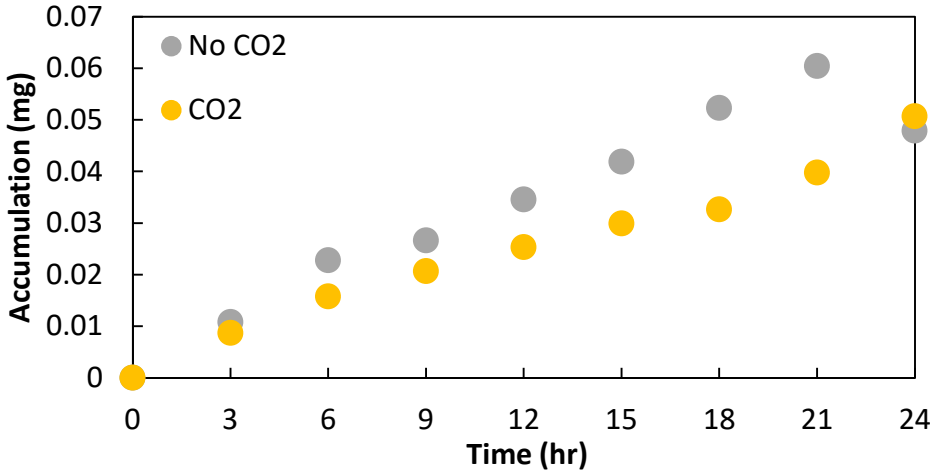

Figure 16. Particle build up over 24 hour period for a non-CO_2 and CO_2 system.

As shown, as run time increases, the amount of fouling inside the system increases linearly, as we had expected. However, it is seen that when diffusiophoresis is in effect, less fouling occurs compared to a system with no diffusiophoresis. While this trend demonstrates that diffusiophoresis incurs less fouling, it is a cause of concern based on the size of the system. Due to the CO_2 line only being 40 mm, a small value of accumulation can demonstrate negative impacts for the separation process over time. These impacts can cause the system to stall and stop the process entirely. In addition, particles entering the system may be less responsive to the concentration gradient which would result in the separation efficiency to decrease.

One interesting point on the graph is at the 24 hour mark. After 24 hours, the diffusiophoresis system demonstrated a more accumulation than the non-diffusiophoresis system. This is most likely due to a clog inside the system existing out from the flow of the solution during the non-diffusiophoresis system. This is further supported when observing the pressure over time

graph of the non-diffusiophoresis system shown in Figure 17. The increase in pressure is due to clogs forming in the system so over time, the general trends demonstrated clogs forming inside the system. However, at the 24 hour mark, a decrease in the pressure is shown is which demonstrates the opposite of a clog forming. A clog left the system at the 24 hour mark causing the pressure to decrease. Figure 27 in Appendix B is a pressure over a 18 hour run time that shows a clear trend of clogs forming and leaving the system. Figure 17 does not demonstrate the same trend and approaches higher pressures then Figure 27 due to the CO_2 line shortening for Figure 17 which causes more accumulation to form faster. This situation is likely to occur inside a diffusiophoretic system over time which would lead to the outlet being more contaminated then theoretically be. This could insight a critical point for existing accumulation to be pushed out of the system.

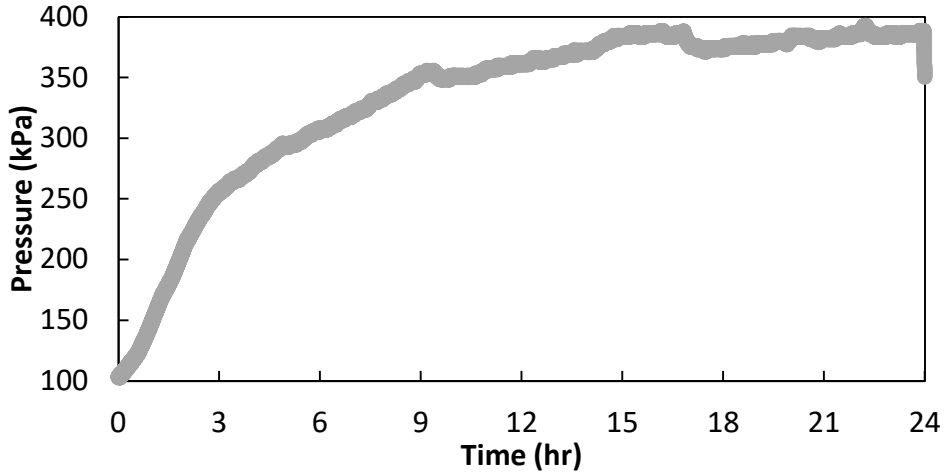

Figure 17. Pressure over time of the non-diffusiophoresis run. A pressure increase represents the formation of a clog in the system and a pressure decrease is due to the loss of a clog exiting out of the system.

In addition to the trend, microscopic images of the CO_2 line after the run support the accumulation inside the system. As shown in Figure 18, an impurity, most likely PS, was seen in the middle of the CO_2 line tubing. From the figure, the size of the impurity was found to be around 1.2 mm meaning that the impurity was the size of a settable particle.[22]

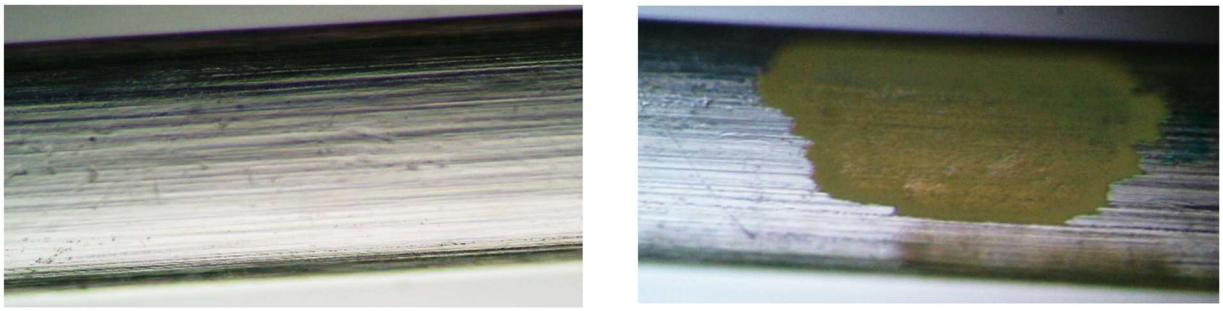

Figure 18. Comparison of CO_2 line before (left) and after (right) running the system. The CO_2 line after the run has a spot of visible build-up, around 1.2 mm long. Where the before image is the CO_2 line after being cleaned in the ultrasonic cleaner.

Cleaning

When developing our initial plans to clean the system and analyze the cleaning outlet, we planned on using toluene as the main solvent to dissolve the polystyrene in the system from the run. When flowing toluene we planned on flowing it through the system at the same amount of time as the initial run and then analyze the total amount of outlet collected under a UV-vis spectrometer similar to Figure 10 with the polystyrene in DI water curve. However, these plots would differ due to Figure 10 focusing on a suspension and utilizing visible light, with a range of 400 nm – 1000 nm, while the UV-vis focused on dissolution and utilizing the UV range of 200 nm – 400 nm. When running toluene under the UV-vis, we focused on a wavelength of 245 nm as this is an expected peak for absorption and molar absorptivity coefficient. While developing a concentration calibration curve, we discovered the issue that toluene and styrene contained the same peak around 245 nm and we would not be able to distinguish a difference between the two compounds. Both toluene and styrene contain benzene as a component in the chemical makeup which would explain why at 245 nm they both have peaks. As a result, we changed our method to utilizing acetone instead of toluene due to acetone not containing benzene and would be able to determine a distinction between solute and solvent.

Before we could begin using acetone, we had to reassure and do research to determine if acetone would be able to dissolve polystyrene. The source assured that polystyrene is soluble in acetone. The polystyrene that was provided to use came from Bang Laboratories Inc. which confirmed the solubility.[27] When mixing acetone with polystyrene styrofoam, our expected results were achieved and observed that acetone and styrene demonstrated different peaks and an easy distinction between the two when running under the UV-vis spectrometer (show figure). Once our confirmations were correct, we began flowing acetone to clean the system and dissolve polystyrene. We then began to start developing a calibration curve by dissolving 0.1 mg of polystyrene beads with 100 mL of acetone to create a 100 mg L^{-1} solution. This value was chosen as higher values would result in absorbances above 1. A stir plate helped mix and constantly stir the polystyrene bead in acetone. The mixer was run for around 8 hours and noticed that the polystyrene did not fully dissolve in the acetone. We then continued to mix the solution the next day for another 8 days and noticed that the somewhat dissolved particles of the bead began to clump together as shown in Figure 19.

Figure 19. 0.1 mg of polystyrene (bead) in 100 mL of acetone solution after 16 hours of mixing. The white substance in the middle of figure was the bead which had deformed and most likely formed napalm which is the product of mixing polystyrene and acetone.

From this analysis we determined that the substance we had be mixing was napalm due to its texture and chemical reaction. In addition to the reaction, we believe that the molecular weight of

the polystyrene may have caused some issues and caused partial dissolution to occur. We then attempted to test another form of polystyrene that had been used to create a 411.67 NTU stock solution of polystyrene in water in the lab. We had taken 0.1 mg of the dry polystyrene and placed it in 100 mL of acetone to replicated the same settings as 0.1 mg polystyrene bead in 100 mL of acetone. The stir plate was used once again and demonstrated similar results as shown in Figure 20.

Figure 20. 0.1 mg of polystyrene (dry) in 100 mL of acetone solution after an hour of mixing. From this chemical reaction, napalm is created which is a rubberish substance.

As a result of this discovery, we determined that polystyrene was not readily soluble in acetone and that more acetone was needed to dissolve the bead and dry forms of polystyrene so that the solubility was met. In addition the solubility issues, another issue that occurred was the motor stalling when running acetone through the system for more than an hour. When flowing acetone through the system as an attempt to clean the system, the pump would stall due to the O-ring on the syringe deforming from the acetone sitting in the syringe as shown in Figure 21.

Figure 21. Deformed O-ring on metal syringe after letting acetone sit for an hour.

After noticing the deformation, we had stopped using the syringe and noticed that the O-ring had gone back to its original shape, most likely due to the acetone evaporating over time. By utilizing Harvard Apparatus stainless steel syringes, research into the replacement part found that the part was sold separately from the company.[28] Further research discovered that the O-rings the syringes had been using would not be adequate for chemicals such as acetone and toluene.[29] This development further proved that cleaning the system with chemical solvents would not be the most ideal cleaning process. Based on these discoveries, we determined that flowing acetone through the system would be an inefficient cleaning process due to the amount of acetone needed to dissolve 0.1 mg of polystyrene, the cleaning process would require hours/days of acetone flowing through the system, and stalling would occur.

In an attempt to determine another chemical to dissolve polystyrene, we utilized ethanol/isopropyl alcohol to try and dissolve the polystyrene beads. However, when leaving the beads to sit in the solvent for around 20 minutes with stirring, we noticed that the beads did not change shape or texture. This resulted in changing our cleaning process entirely as seeing that no chemical solvent would be efficient enough to clean the system and collect data.

Without the use of a chemical solvent to clean the system, we relied on the use of an ultrasonic cleaner and compressed air. The ultrasonic cleaner utilized sound vibrations to help clean and allow contaminants in the tube to cavitating out. Once the water line was in the ultrasonic cleaner for an estimated hour, we would flow distilled water through the tube and then flow compressed air to ensure that any leftover particles would be wet and easy to flow out from the air. This method was effective for cleaning the system as no visible accumulation could be seen inside the water line when examined under a microscope as shown in Figure 22. The water line used in the ultra-sonic cleaner contained the least amount of impurities. Additionally, Figure 18

also shows the effectiveness of the ultrasonic cleaner as it compares the before and after microscopic images of the CO_2 line.

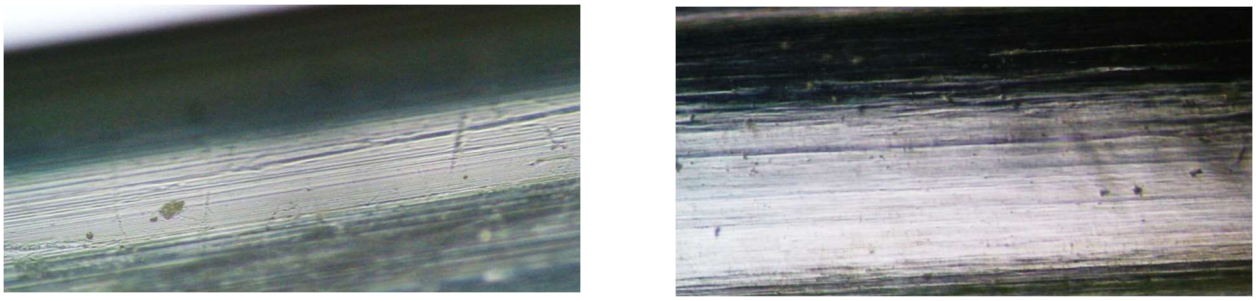

Figure 22. Comparison of water line before the run (left) and water line after the ultra-sonic cleaning (right). Water line was left in the ultra-sonic cleaner for 1 hour. DI water and air were then flown through the tubing to remove any excess water from the cleaner.

The only complication that came about was the removal and reassembling of the system. We had to remove the water line and detach the ferrules constantly when having to clean the line. The system was not 100% the same for each run but we assured that no leaking and no water build up occurred in the junctions before an experiment was conducted by running leak tests and blowing compressed air through the system prior to each run.

COMSOL Simulations

Model Construction and Geometry

For the model which simulates the flow path and velocity profile in the gap region on the system, the geometry is simply a cylinder. Such geometry allows for using COMSOL's 2D-axisymmetric geometry since the velocity field varies only radially and axially, and not angularly. The region is modeled as a rectangle, with one of the walls having an axial symmetry, effectively representing the center of the tube. While the opposite wall represents the inner wall of the water line, along with the dimensions of the capillary, as reported in Table 3, the geometry and boundaries were set up in COMSOL. As shown by Lyu[9], the distance between the capillary and the end of the CO_2 line affects flow patterns and particle movement in the region. For the purpose of the model, it was set up to have a distance of 1 mm, though this can be easily changed in the geometry for future models.

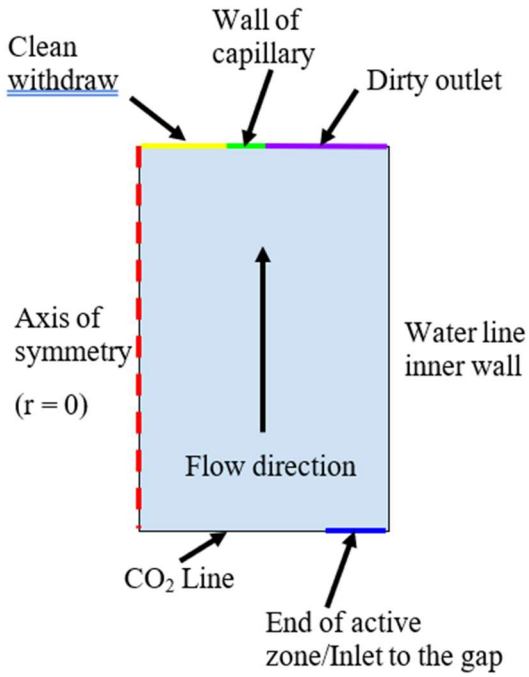

Figure 23. Schematics of the COMSOL model where the axis of symmetry represents the center of the tube, capillary, wall of the capillary, and the dirty outlet labeled.

First, general parameters were defined, such as the flowrate set on the inlet pump, the area of the flow path in the active zone, between the outer wall of the CO_2 line and the inner wall of the water line, and the average velocity of the inlet flow can then be calculated. The inlet flowrate used for this simulation was set to be 75 μL/min, as this is a general number that previous studies have shown to be of Additionally, a parameter called "split ratio" is defined, as a variable that controls the ratio between the clean withdraw and total input, for this model, it is set to 0.2, meaning the withdraw flowrate is effectively 20% of the inlet flowrate. COMSOL also allows for material definition in the domain, which, in this case, was set to be water.

Table 5. Summary of parameters used and operating conditions used for this simulation.

Length of gap	Flowrate	Split Ratio
1 mm	75 μL/min	0.2

Physics Packages

Since the gap region is immediately after the active zone where diffusiophoresis occurs, the only force driving the flow is the drag force in the domain from the pump pushing flow through the system. Additionally, we wish to obtain the simulated flow path of particles. Thus, the only physics needed for this model in COMSOL is the Laminar Flow and Particle Tracing for Fluid Flow physics packages.

Laminar Flow

The Laminar Flow package is used to simulate the flow and velocity profile in the system, the main governing equation is shown below.

$$\rho\left(\frac{\partial u}{\partial t}+u\cdot\nabla u\right)=-\nabla p+\nabla\cdot\left(\mu(\nabla u+(\nabla u)^{T})-\frac{2}{3}\mu(\nabla\cdot u)I\right)+F \qquad (12)$$

Where u is the fluid velocity, ρ is the fluid density, μ is the fluid dynamic viscosity, p is the fluid pressure, and F is the sum of external forces. In this equation, the left-hand side

corresponds to the inertial forces, while the first term on the right-hand side (pressure gradient term) is to pressure forces, the third term is viscous forces and the fourth term is the external forces. As mentioned above, the material in the domain has been defined as water and fluid properties such as density and viscosity are taken from the material data. In this case, the external forces term can be taken out of the equation as it is zero. The velocity profile is at steady state, so the velocity does not change with changing time. Initially, there is no movement in the domain, thus, the initial velocity is zero in all directions.

In term of boundary conditions, since the model is built in COMSOL's 2D-axisymetric mode to represent a cylindrical coordinate system, there is a natural axial symmetry boundary condition which is at r = 0 which represents the center of the tube as shown in Figure 13. At the inlet, the boundary condition is defined as fully developed flow, with an average velocity calculated from the known inlet flow rate and active zone flow area. This is also justified by approximations for entry length, that is, the distance it takes before the flow profile becomes fully developed for a set of operating conditions and system geometry. For the dirty outlet shown in Figure 13, the boundary condition applied is a static pressure, which is the liquid pressure in the system, maintained by the back pressure regulator, for this model, has a value of 160 kPa. For the clean withdraw, the boundary condition is defined as velocity, calculated using known tube dimensions, inlet flowrate, and split ratio as mentioned previously. Lastly, all other boundaries, including the inner wall of the water line, the wall of the capillary, and the end of the CO_2 line were kept as walls and had no slip boundary conditions (velocity is 0 at these boundaries).

Particle Tracing for Fluid Flow

The Particle Tracing for Fluid Flow package is used to track particles of desired properties in the domain. The main governing equation is shown below.

$$\frac{d}{dt}(m_p \boldsymbol{v}) = \boldsymbol{F}_t \quad (13)$$

Where m_p is the particle mass, $\boldsymbol{v}$ is the particle velocity represented as a vector, and $\boldsymbol{F}_t$ is the sum of forces present or acting on the system. In this case, the only force in effect is the drag force caused by the flow in the system. The drag force equation is shown below.

$$\boldsymbol{F}_D = \frac{18\mu}{\rho_p d_p^2} m_p(\boldsymbol{u} - \boldsymbol{v}) \quad (14)$$

Where ρ_p is the particle density, d_p is the particle diameter, and $\boldsymbol{u}$ is the velocity field of flow in the domain. As the sample solution used in our experiments was water with suspended polystyrene, the particles are in solid form, and settings were changed accordingly. Particle properties such as the density and diameter were obtained from Bangs Laboratory (PS03001), who supplied the stock solutions.

As the flow package was solved first, the solution of the flow velocity field was kept and used in calculations of particle tracing. The two packages were linked to account for the velocity field in the domain, as for the drag force term and initial velocity. At both the clean withdraw and dirty outlet, the boundary conditions are set to freeze, meaning once the particles reach there, they will just stick and stay there. While the end of the CO_2 line, inner wall of the water line, and the wall of the capillary all have boundary conditions set to bounce, meaning particles will bounce at the same deflection angle as the angle of attack approaching the walls. Lastly, the axial symmetry also had a boundary condition of bounce. This implies that at the point where a particle hits the axis at r = 0, or the center of the tube, there is another particle coming in with the same attack angle, crossing r = 0 at the exact same location. We deemed this assumption to be appropriate as runs of the simulation suggested the chances of particles even hitting the axis of symmetry under

conditions that were used to be very low. Lastly, there were also options to control the number of particles to be released, time to be released, and initial distribution of particles along the inlet. These settings were changed throughout the studies.

Mesh

COMSOL Multiphysics is a software that interconnects simulations of various physical phenomena using the finite element method (FEM). FEM is a commonly used mathematical analysis method to solve engineering problems, mostly boundary value problems, that would otherwise be much more difficult to solve. FEM essentially divides up the domain of interest into much smaller pieces, which are called finite elements, based on particular space discretization and dimensions. FEM approximates the unknown function in each one of the smaller domains, then they are put together to form the original domain. The approximation of solution is done by minimizing an associated error function via variation methods.[30]

In COMSOL, we can control the shape, size, distribution, scale, and refinement of said finite elements. In most cases, leaving the mesh as physics-controlled will work, but for more complicated models, or to minimize error accumulated in the process of solving, the mesh may be refined in any of the ways mentioned above. From prior experience with COMSOL, it is common to see the edges and corners near inlets and outlets of a system involving flow to be particularly large contributors to inaccuracy. Thus, distributions were added to focus on these areas, along with corner refinements. Meaning the mesh size in these areas would be smaller than the middle of the domain, in order to keep the total number of domains to a reasonable range, while focusing smaller mesh sizes in areas where high error is often observed. Lastly, free triangulars were added, changing the finite elements' shape to triangles from the default quads. As doing so also lowered the number of elements while maintaining the same level of accuracy, as observed through using

various meshes. The resulting mesh and the one used for the simulation with all results reported are shown below as Figure 24. Such mesh yielded 8246 domain elements and 262 boundary elements.

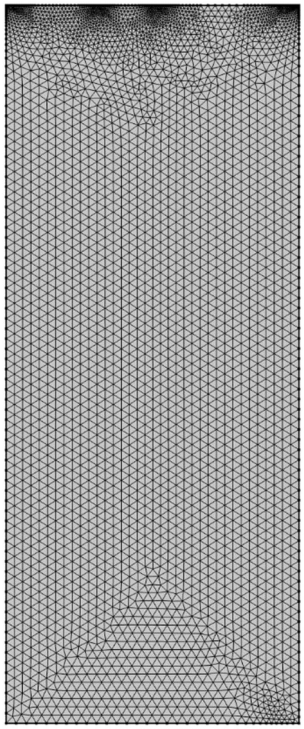

Figure 24. Final mesh used in COMSOL with modifications with distribution near inlet and outlets, ratio of 1.2, corner refinement around the inlet and outlets, free triangular meshes, and finer mesh sizes.

Results

The main result from this simulation is obtaining the velocity profile and flow path in the gap region. A concern prior to the completion of the simulation was the possibility of particles mixing in this region or having turbulence in the flow path caused by the sudden expansion in flow path. If that were true, then the separation of particles achieved as a result of diffusiophoresis in the active zone would be gone. Then the solution withdrawn from the system would be the same, or close to, the initial concentration. As our results show (Figure 25), with the conditions that the simulation was completed under, the concerns are proven to be irrelevant. Much higher flowrates, and therefore velocity in the active zone would be needed to see any significant changes to the

velocity field and particle trajectories. With a higher flowrate, a much longer system would be needed to maintain the same residence time, and thus effects of separation, which may be unrealistic. Additionally, high flowrates also pose a risk to the tubing itself as the material of Teflon AF-2400 is quite fragile.

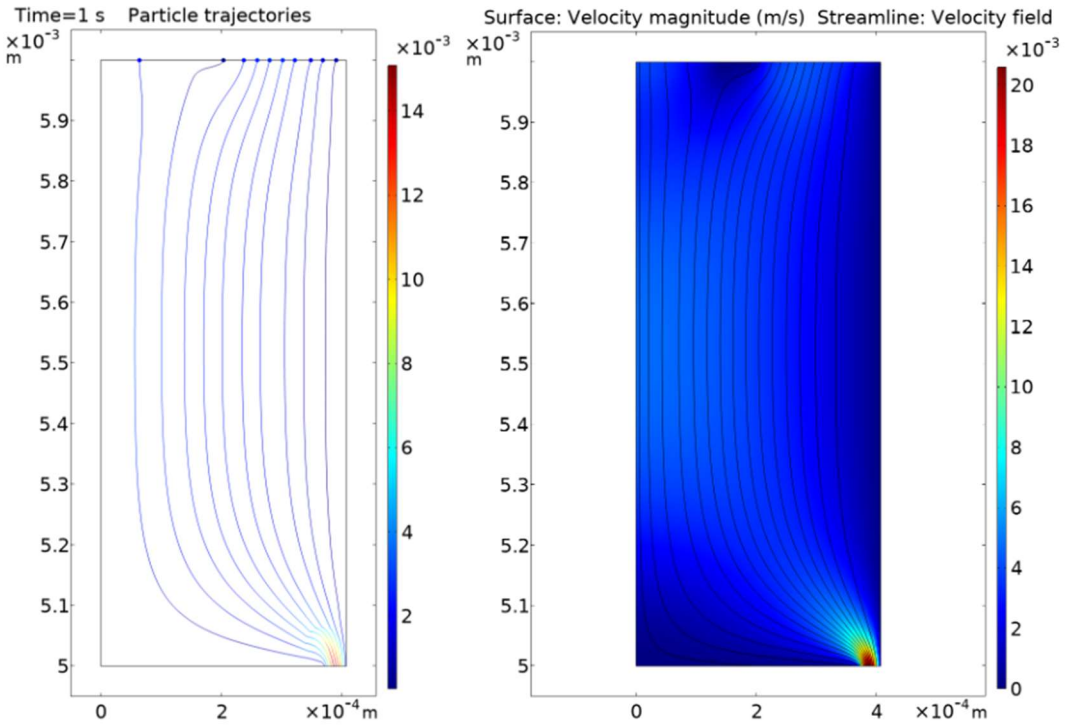

Figure 25. The particle trajectories of 10 particles being released at t = 0 and with uniform distribution along the inlet (left). The surface plot of the velocity field in the domain with streamlines shown (right).

The other main result from these simulations is to study the split between the number of particles that end up in the clean withdraw, as well as the dirty outlet. To do this, the clean withdraw and dirty outlet were divided up into smaller equidistant segments. Doing so would allow us to find the number of particles that are at each smaller segment at the end of the simulation and graph the results with respect to radial position. This simulation was run twice, once with 50,000 particles released, and the other with 100,000 particles released. The result for the split between the clean withdraw and dirty outlet can be found below as reported in Table 6.

Table 6. Reported values of initial particles released, resulting number of particles at the clean withdraw and dirty outlet and percentages for both.

Initial	Clean withdraw	Clean withdraw (% of initial)	Dirty outlet	Dirty outlet (% of initial)	Total at both outlets	Total at both outlets (% of initial)
50,000	7,333	14.67	42,658	85.32	49,991	99.98
100,000	14,664	14.67	85,316	85.33	99,980	99.98

As the results show, almost all of the particles released in this case reached one of the outlets. The ones missing may be due to errors in the calculation methods, or due to the simulations not being run for long enough. However, the missing particles were not due to particles being stuck at the walls, which would imply the possibility of fouling and build-up on the walls. As the walls were also analyzed at the end of each run and no particles were present on those boundaries. In terms of the normalized split in percentages in the two runs, they are almost identical, which shows the reproducibility and reliability of the model. With a split ratio of 0.2, that is, the clean withdraw pulling at a flowrate that is 20% of the inlet flowrate, the percentage of particles ending up in the clean withdraw is roughly 14.67%.

Next, the number of particles were plotted against the radial position of the shorter equidistant segments to show the particle distribution across the two outlets (Appendix B, Figures 28, 29). The data were then normalized by converting into percentage of the total number of particles released, the two runs were then overlayed, resulting in Figure 26.

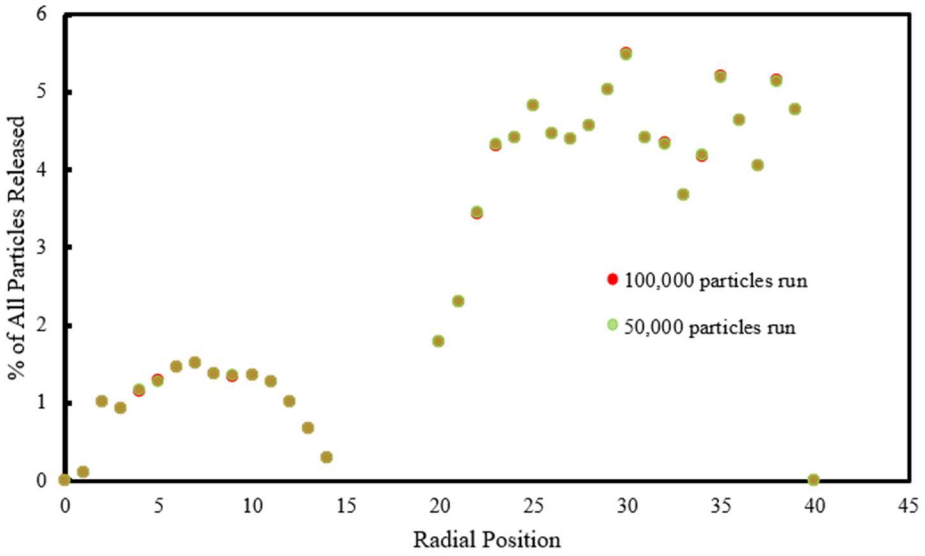

Figure 26. Normalized % of all particles released plotted against radial position in the gap region.

As Figure 26 shows, the trend between the two runs is identical, which is to be expected. With the two runs' only difference being the number of particles, all other settings and mesh remained the same. Therefore, it would make sense for the two runs to have the same degrees of error in calculation and noises present. However, the trend in general did not match our initial expected results. We were expecting flat lines across both the clean withdraw and dirty outlet showing an equal number of particles in each of the shorter segments across each of the outlets. As we took into consideration the sudden expansion in flow path, velocity field we obtained, and presence of the capillary wall, we made sense of why the number of particles is lower near the walls with no slip boundary conditions. Additional plots of the two runs reported as number of particles vs. radial position can be found in Appendix B.

For the purpose of these simulations, the particles released at the inlet were distributed radially across the inlet uniformly. In the presence of diffusiophoresis, this would be an inaccurate assumption as the particles should move in response to the concentration gradient of hydrogen ions present in the active zone. Which means, by the end of the active zone, or the inlet to the gap

region, the particles should not be distributed uniformly but rather from a concentration gradient radially. Such initial particle distribution to the gap region would result in a different result of particle distribution at the outlets of the gap than that shown in Figure 26. However, this has no effect on the flow pattern and streamlines. The results showed that for a uniform distribution of particles, the method of separation proved to be valid as it can effectively pull water at a relatively lower concentration out of the center of the tube. In the presence of diffusiophoresis, the concentration of particles is expected to be higher closer to the inner wall of the water line. Which, according to our simulated results, would result in an even more effective separation as the concentration difference in the clear withdraw and dirty outlet would be even greater than that shown in Figure 26. Additionally, the gap region model also shows the effects of the sudden expansion on streamlines, which may eventually be used to predict accumulation in the gap region at various sets of parameters and geometries.

Conclusions and Recommendations

Fouling

Through analysis of system accumulation with active and inactive diffusiophoresis, we found that while both conditions yielded relatively constant accumulation over a 24-hour period, when diffusiophoresis was active in the system, there was less accumulation over time. This indicates that including diffusiophoresis should not cause increasing concern for the functionality of the system, however, the system will need some form of maintenance to remove accumulation. As we discovered in our experiments, simple rinsing methods with common solvents do not successfully clean the system. Deconstructing the system for thorough cleaning or part replacements defeats the purpose of the continuous system which leaves room for further research to develop a method for maintaining the assembled system. Additionally, further research must be conducted to determine if the amount of fouling occurring has a significant effect on the effectiveness of the systems separation and product.

Mixing of Particles and Disturbances to Flow in the Gap Region

In conclusion, we've shown that there is no mixing or turbulence in the flow pattern as a result of our operation conditions or the nature of the sudden expansion in the flow path. We were able to obtain the flow velocity profile and particle trajectories, where this information can be used to predict fouling on the walls of the active zone in the presence of diffusiophoresis. Additionally, we've shown the theoretical distribution of particles radially across both the clean withdraw as well as the dirty outlet. While also showing the split between clean withdraw and dirty outlet for our set of operating conditions as shown in Table 6.

Recommendations for Future Works

After learning the difficulties of assembling and running experiments with the diffusiophoretic water separation system, we had learned a few important takeaways about how to run future experiments and real world implementation. For future experiments, when assembling the system, it is important to utilize tools that will ensure the tubing and system parts will not break and cause leaks. Due to the expectation of fouling to occur within the flow cell when it is attached to the outlet, it is advised to place the flow cell over the water line, right above the end of the CO_2 line and seal end. However, a technique to ensure that the water line is centered in the flow cell should be furthered analyzed. For cleaning purposes, the use of chemical solvents such as toluene and acetone are not viable if the solvents are flown through the system for long periods of time for an effective cleaning. The best method to clean the system involves the use of distilled water and the ultrasonic cleaner to clear the debris from the water line. Once the ultrasonic cleaner is done, flow distilled water and air to remove and water and debris left from the cleaner. For future research into fouling in the system, various system changes should be made such as changing the residence time, length of the diffusiophoretic active zone, and the CO_2 pressure. For each of these changes, a system with no diffusiophoresis should be measured as well for comparison. In addition, a method to determine fouling over time and develop a new and efficient cleaning method in order to develop more accurate transient data. For real world implementation, the system used would not be efficient due to the process having a long run time in which fouling occurs with little clean outlet. However, with scale-up, it is possible that less leakage could occur and separation would increase with increased tubing.

We believe the COMSOL model of the gap region has proved our hypothesis, which stated that there was no mixing of particles in the gap region of the system, under the current operating conditions. However, as it can be seen in Figure 26 there are some discontinuities near the walls

of the system, this may be close to the actual flow profile, or it may be due to boundary conditions set in the model. It may be worth further investigation to improve the model and its accuracy. On top of prior work by Lyu[9], there has been a COMSOL model of the active zone with the chemical reactions added into it. That model can now show us the gradient of not only CO_2 but also all other species that are present in the domain as a result of the CO_2 reacting with water. In the future, the theoretical charged particle movement in response to fluid flow, the concentration gradients, and electric field present in the system should also be tracked. Doing so would allow for predictions of theoretical results of particle separation. Lastly, further mesh refinement may also prove to be beneficial as that would both improve efficiency and accuracy of results.

References

(1) Shiklomanov, I. A. Appraisal and Assessment of World Water Resources. *Water Int* **2000**, *25* (1), 11–32. https://doi.org/10.1080/02508060008686794.

(2) Sharma, S.; Bhattacharya, A. Drinking Water Contamination and Treatment Techniques. *Applied Water Science*. Springer Verlag June 1, 2017, pp 1043–1067. https://doi.org/10.1007/s13201-016-0455-7.

(3) Guha, R.; Shang, X.; Zydney, A. L.; Velegol, D.; Kumar, M. Diffusiophoresis Contributes Significantly to Colloidal Fouling in Low Salinity Reverse Osmosis Systems. *J Memb Sci* **2015**, *479*, 67–76. https://doi.org/10.1016/j.memsci.2015.01.024.

(4) Shin, S.; Shardt, O.; Warren, P. B.; Stone, H. A. Membraneless Water Filtration Using CO2. *Nat Commun* **2017**, *8*. https://doi.org/10.1038/ncomms15181.

(5) Shim, S.; Baskaran, M.; Thai, E. H.; Stone, H. A. CO2-Driven Diffusiophoresis and Water Cleaning: Similarity Solutions for Predicting the Exclusion Zone in a Channel Flow. *Lab Chip* **2021**, *21* (17), 3387–3400. https://doi.org/10.1039/d1lc00211b.

(6) Shim, S.; Stone, H. A.; Weitz, D. A. CO 2-Leakage-Driven Diffusiophoresis Causes Spontaneous Accumulation of Charged Materials in Channel Flow. *PNAS* **2010**, *117*. https://doi.org/10.1073/pnas.2010011117/-/DCSupplemental.y.

(7) Shimokusu, T. J.; Maybruck, V. G.; Ault, J. T.; Shin, S. Colloid Separation by CO2-Induced Diffusiophoresis. *Langmuir* **2020**, *36* (25), 7032–7038. https://doi.org/10.1021/acs.langmuir.9b03376.

(8) Ault, J. T.; Shin, S.; Stone, H. A. Diffusiophoresis in Narrow Channel Flows. *J Fluid Mech* **2018**, *854*, 420–448. https://doi.org/10.1017/jfm.2018.618.

(9) Lyu, S. *Membraneless Water Purification via Diffusiophoresis*; 2019.

(10) Shin, S.; Ault, J. T.; Warren, P. B.; Stone, H. A. Accumulation of Colloidal Particles in Flow Junctions Induced by Fluid Flow and Diffusiophoresis. *Phys Rev X* **2017**, *7* (4). https://doi.org/10.1103/PhysRevX.7.041038.

(11) Lee, H.; Kim, J.; Yang, J.; Seo, S. W.; Kim, S. J. Diffusiophoretic Exclusion of Colloidal Particles for Continuous Water Purification. *Lab Chip* **2018**, *18* (12), 1713–1724. https://doi.org/10.1039/c8lc00132d.

(12) Velegol, D.; Garg, A.; Guha, R.; Kar, A.; Kumar, M. Origins of Concentration Gradients for Diffusiophoresis. *Soft Matter* **2016**, *12* (21), 4686–4703. https://doi.org/10.1039/c6sm00052e.

(13) Zhang, J.; Teixeira, A. R.; Zhang, H.; Jensen, K. F. Determination of Fast Gas-Liquid Reaction Kinetics in Flow. *React Chem Eng* **2020**, *5* (1), 51–57. https://doi.org/10.1039/c9re00390h.

(14) Zhang, J.; Teixeira, A. R.; Zhang, H.; Jensen, K. F. Automated in Situ Measurement of Gas Solubility in Liquids with a Simple Tube-in-Tube Reactor. *Anal Chem* **2017**, *89* (16), 8524–8530. https://doi.org/10.1021/acs.analchem.7b02264.

(15) Pinnau, I.; Toy, L. G. *Gas and Vapor Transport Properties of Amorphous Perfluorinated Copolymer Membranes Based on 2,2-Bistrifluoromethyl-4,5-Difluoro-l,3-Dioxole/Tetrafluoroethylene*; 1996; Vol. 109.

(16) O'Brien, M.; Taylor, N.; Polyzos, A.; Baxendale, I. R.; Ley, S. V. Hydrogenation in Flow: Homogeneous and Heterogeneous Catalysis Using Teflon AF-2400 to Effect Gas-Liquid Contact at Elevated Pressure. *Chem Sci* **2011**, *2* (7), 1250–1257. https://doi.org/10.1039/c1sc00055a.

(17) Alentiev, A. Y.; Shantarovich, V. P.; Merkel, T. C.; Bondar, V. I.; Freeman, B. D.; Yampolskii, Y. P. Gas and Vapor Sorption, Permeation, and Diffusion in Glassy Amorphous Teflon AF1600. *Macromolecules* **2002**, *35* (25), 9513–9522. https://doi.org/10.1021/ma020494f.

(18) Firpo, G.; Angeli, E.; Repetto, L.; Valbusa, U. Permeability Thickness Dependence of Polydimethylsiloxane (PDMS) Membranes. *J Memb Sci* **2015**, *481*, 1–8. https://doi.org/10.1016/j.memsci.2014.12.043.

(19) *Amorphous Fluoroplastic Resins Product Information*; 2016. www.fluoropolymers.org.

(20) Browne, D.; O'Brien, M.; Koos, P.; Cranwell, P. B.; Polyzos, A.; Ley, S. V. Continuous-Flow Processing of Gaseous Ammonia Using a Teflon AF-2400 Tube-in-Tube Reactor: Synthesis of Thioureas and in-Line Titrations. *Synlett* **2012**, *23* (9), 1402–1406. https://doi.org/10.1055/s-0031-1290963.

(21) Jonquiè, A.; Clément, R.; Lochon, P. *Permeability of Block Copolymers to Vapors and Liquids*. www.elsevier.com/locate/ppolysci.

(22) Guo, W.; Ngo, H. H.; Li, J. A Mini-Review on Membrane Fouling. *Bioresour Technol* **2012**, *122*, 27–34. https://doi.org/10.1016/j.biortech.2012.04.089.

(23) Shin, S.; Ault, J. T.; Warren, P. B.; Stone, H. A. Accumulation of Colloidal Particles in Flow Junctions Induced by Fluid Flow and Diffusiophoresis. *Phys Rev X* **2017**, *7* (4). https://doi.org/10.1103/PhysRevX.7.041038.

(24) Rocha, F. S.; Gomes, A. J.; Lunardi, C. N.; Kaliaguine, S.; Patience, G. S. Experimental Methods in Chemical Engineering: Ultraviolet Visible Spectroscopy-UV-Vis. The Canadian Journal of Chemical Engineering 2018, 96 (12), 2512–2517.

(25) Niemczewski, B. Observations of Water Cavitation Intensity under Practical Ultrasonic Cleaning Conditions. *Ultrason Sonochem* **2007**, *14* (1), 13–18. https://doi.org/10.1016/j.ultsonch.2005.11.009.

(26) Korea, J. &. *AMERICAS & WORLD HEADQUARTERS EUROPE, MIDDLE EAST & AFRICA Trademarks Limit of Liability*; 2013. www.oceanoptics.com.

(27) *Common Solvents and Non-Solvents of Polystyrene*. www.bangslabs.com.

(28) *Stainless Steel Syringe Replacement Fittings*. https://www.harvardapparatus.com/stainless-steel-syringe-replacement-fittings.html (accessed 2023-04-22).

(29) *Viton Chemical Compatibility*. https://www.calpaclab.com/viton-chemical-compatibility-chart/ (accessed 2023-04-22).

(30) Hanna, O. T.; Sandall, O. C. *Computational Methods in Chemical Engineering*; Prentice-Hall, Upper Saddle River, NJ , 1995.

Appendix A - Calculations

A.1: Volume of CO_2 Line

$$V_{CO2,ID} = \pi \left(\frac{D_{CO2,ID}}{2}\right)^2 L$$

$$V_{CO2,ID} = \pi \left(\frac{0.6096\ mm}{2}\right)^2 (40\ mm)$$

$$V_{CO2,ID} = 11.67\ mm^3$$

A.2: Volume of Water Line

$$V_{H2O,ID} = \pi \left(\frac{D_{H2O,ID}}{2}\right)^2 L$$

$$V_{H2O,ID} = \pi \left(\frac{0.8128\ mm}{2}\right)^2 (40\ mm)$$

$$V_{H2O,ID} = 20.75\ mm^3$$

A.3: Water Volume

$$V_{H2O} = V_{H2O,ID} - V_{CO2,ID}$$

$$V_{H2O} = 20.75\ mm^3 - 11.67\ mm^3$$

$$V_{H2O} = 9.08\ mm^3 = 9.08 * 10^{-9}\ m^3$$

A.4: Solution Flow Rate

$$t_{res} = 75\ s$$

$$F = \frac{V_{H2O}}{t_{res}} = \frac{9.08 * 10^{-9}\ m^3}{75\ s} * \frac{60\ s}{1\ min} * \frac{1 * 10^6\ mL}{1\ m^3} * \frac{1000\ \mu L}{1\ mL}$$

$$F = 7.26\ \frac{\mu L}{min}$$

A.4: Beer-Lambert Law

The data selected is for the no CO_2 run at the 21 hour sample. The wavelength of the intensities are at 356.819 nm. This equation was performed for every sample and every wavelength.

$$I_{sample} = 7917.61, I_{background} = 304.82, I_{reference} = 22217.25$$

$$A = -\log\left(\frac{I_{sample} - I_{background}}{I_{reference} - I_{background}}\right)$$

$$A = -\log\left(\frac{7917.61 - 304.82}{22217.25 - 304.82}\right)$$

$$A = 0.46$$

A.5: Mass Balance

$$Inlet - Oulet = Accumulation$$

$$F_{in}x_{in} - F_{out}x_{out} = \frac{dM}{dt}$$

$$F = F_{in} = F_{out}$$

$$F(x_{in} - x_{out}) = \frac{dM}{dt}$$

$$F\int_0^t (x_{in} - x_{out})dt = \int_0^M dM$$

$$Ft(x_{in} - x_{out}) = M$$

Appendix B – Additional Plots

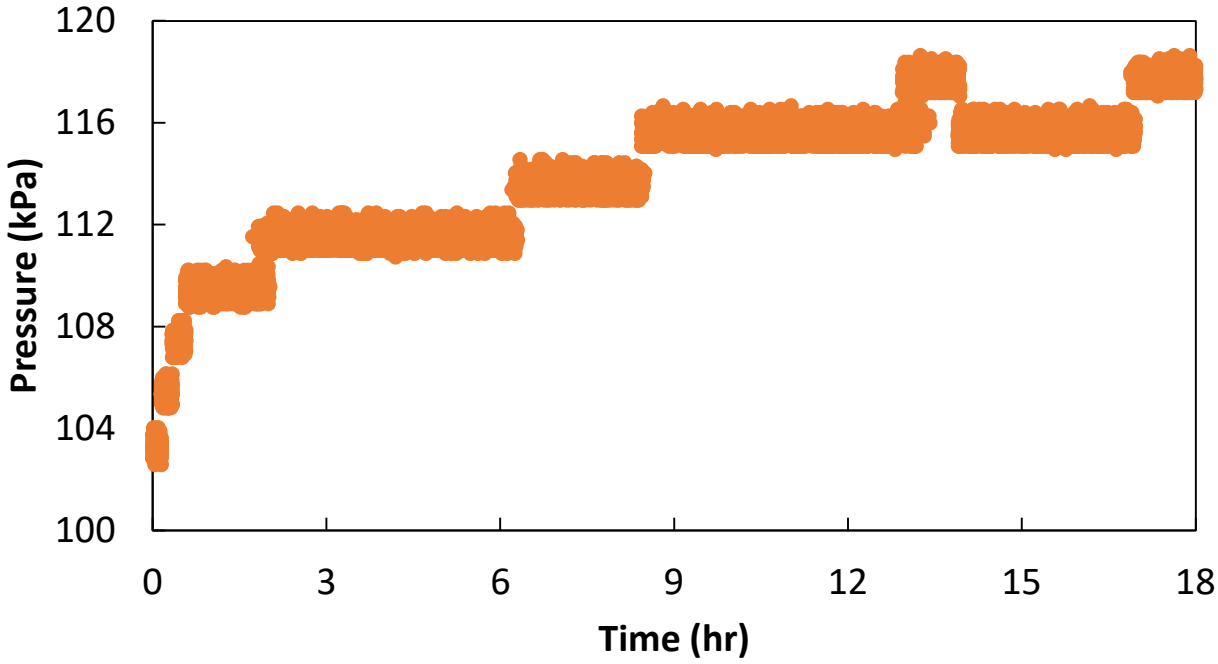

Figure 27. Pressure data of a no CO_2 run over 18 hour run time. Clearly shows pressure staying constant and then increasing over time demonstrating the formation of clogs over time. The decrease in pressure represents a clog leaving the system.

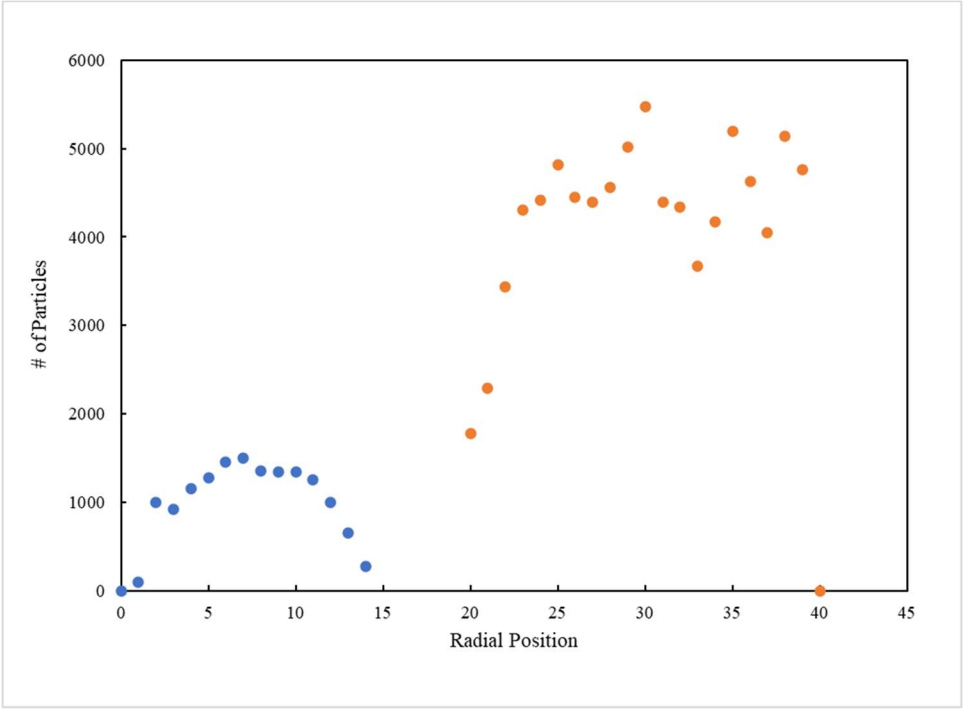

Figure 28. The number of particles across the outlets plotted against the radial position with an initial release of 100,000 particles.

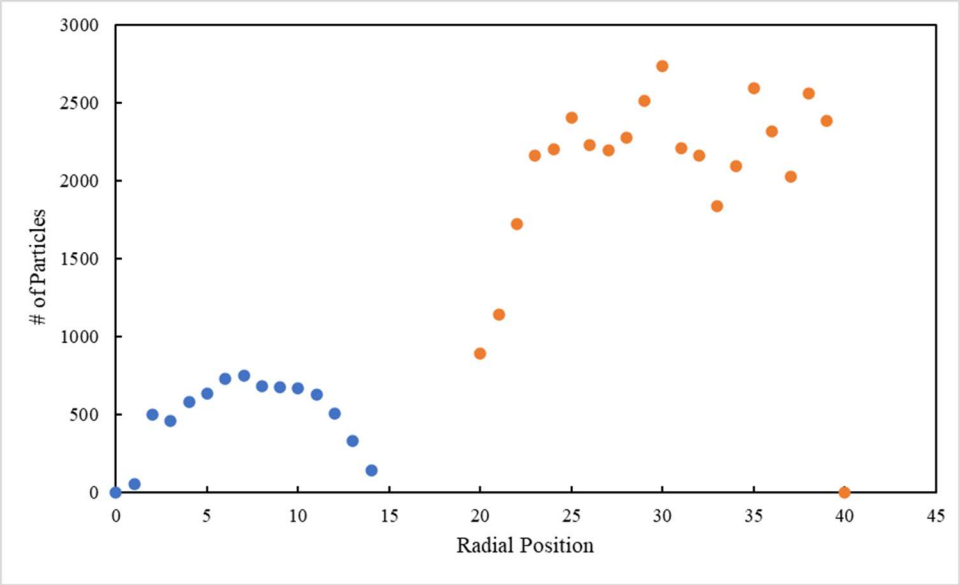

Figure 29. The number of particles across the outlets plotted against the radial position with an initial release of 50,000 particles.

Appendix C – Additional Tables

Table 7. Absorbance and outlet concentration data for no CO2 run at a wavelength of 356.819 nm. The outlet concentration was converted to accumulation with the use of the mass balance to create Figure 16.

Time (hr)	Absorbance	Outlet Concentration (mg^1L^{-1})
0	0.50	20.27
3	0.44	17.72
6	0.43	17.45
9	0.48	19.37
12	0.46	18.41
15	0.46	18.54
18	0.44	17.81
21	0.46	18.36
24	0.58	23.22

Table 8. Absorbance and outlet concentration data for CO2 run at a wavelength of 356.819 nm. The outlet concentration was converted to accumulation with the use of the mass balance to create Figure 16.

Time (hr)	Absorbance	Outlet Concentration (mg^1L^{-1})
0	0.44	52.52
3	0.38	45.85
6	0.39	47.12
9	0.40	48.79
12	0.41	48.95
15	0.41	49.04
18	0.42	50.44
21	0.39	47.04
24	0.37	44.20